Winter 12-2017

VISCOELASTIC BEHAVIOR OF CARBON FIBER REINFORCED POLYMER COMPOSITES INCORPORATING NANOMATERIALS

Amy R. Garner

Amy Rachelle Garner

Candidate

Civil Engineering

Department

This thesis is approved, and it is acceptable in quality and form for publication:

Approved by the Thesis Committee:

Dr. Mahmoud Reda Taha , Chairperson

Dr. Walter Gerstle

Dr. Yu-Lin Shen

VISCOELASTIC BEHAVIOR OF CARBON FIBER REINFORCED POLYMER COMPOSITES INCORPORATING NANOMATERIALS

By

AMY RACHELLE GARNER

BACHELORS OF SCIENCE, CIVIL ENGINEERING

THESIS

Submitted in Partial Fulfillment of the
Requirements for the Degree of

Master of Science
Civil Engineering

The University of New Mexico
Albuquerque, New Mexico

December, 2017

DEDICATION

To my loving and caring family for their constant support throughout graduate school. Thank you for always believing in me and encouraging me to chase my dreams.

ACKNOWLEDGEMENTS

I would first like to extend gratitude to my advisor Dr. Mahmoud Reda Taha. Your technical expertise, creativity, and guidance was invaluable towards my success in graduate school. An additional thank you to my committee members, Dr. Yu-Lin Shen and Dr. Walter Gerstle. Thank you for providing your time to serve on my committee and providing insightful feedback. I would also like to extend a special thank you to Michael Peterson and Mark Scherbarth from the Air Force Research Labs and the entire UNM AFOSR Research Team – Dr. Arafat Khan, Elisa Borowski, and Jeremiah Leyba. Thank you for your help in the lab, asking questions, and helping me understand concepts.

I would like to extend my thanks to Mr. Kenny Martinez. Thank you for a constant supply of blue tape, super glue, and laughter. Lastly, thank you to my fellow research group members. I will always appreciate your help in both classes and research work. You are some of the hardest working, insightful, and kind people I have ever been so fortunate to meet.

Preface

During the course of this thesis, the following papers have been submitted for publication in reviewed proceedings.

Garner, A., Genedy, M., Tarefder, R., Reda Taha, M., 2015, "Monitoring Fatigue Damage in PC using Carbon Nanotubes," Advanced Materials Research, 1129, pp.94-101

Garner, A., Khan, A., Reda Taha, M., 2015, "Effect of MWCNTs on Creep of Epoxy for CFRP Deployable Composites," American Society of Composites 30th Technical Conference, East Lansing, MI.

Garner, A., Khan, A., Kandil, U, Soliman, E., Reda Taha., M., "Off-axis Stress Relaxation of CFRP incorporating Alumina Nanoparticles." Submitted to Journal of Composite Materials.

In Preparation

Garner, A., Genedy, M., Reda Taha, M., "Engineering the Viscoelastic Behavior of CFRP Incorporating Multi-Walled Carbon Nanotubes." Journal of Composites: Part B-Engineering

Viscoelastic Behavior of Carbon Fiber Reinforced Polymer Composites incorporating Nanomaterials

by

Amy Rachelle Garner

B.S. Civil Engineering, University of New Mexico, 2014

M.S. Civil Engineering, University of New Mexico, 2017

ABSTRACT

Carbon fiber reinforced polymer (CFRP) composites are increasingly being used in a variety of industries such as aerospace and infrastructure. It is proposed here that by incorporating nanoparticles into the CFRP composite, one could tailor the viscoelastic or mechanical properties of the composite. This is specifically important in controlling strain energy driven deployments for aerospace applications. In a strain energy driven deployment, the initial deployment acceleration can be too high, causing damage to the payload if not managed. It is key to understand a method for controlling the initial deployment and stiffness of these structures.

This investigation experimentally examines the effect of incorporating alumina nanoparticles (ANPs), non-functionalized multi-walled carbon nanotubes (NF-MWCNTs), and functionalized multi-walled carbon nanotubes (F-MWCNTs) on the off-axis stiffness and stress-relaxation of carbon fiber reinforced polymer (CFRP) composites. Epoxy-nanocomposites incorporating 0.0, 1.0, 2.0, and 3.0 wt.% ANPs; 0.0 0.5, 1.0, and 1.5 wt. % NF-MWCNTs; 0.0 0.5, 1.0, and 1.5 wt. % F-MWCNTs of the total weight of epoxy are

examined. Off-axis tension stiffness and stress-relaxation tests were performed on CFRP coupons fabricated with ANPs-nanocomposites. Dynamic mechanical analysis (DMA) testing of neat epoxy and epoxy nanocomposites incorporating nanomaterials was used to identify the stiffness and relaxation behavior of the epoxy-nanocomposite matrix. Fourier transform infrared spectroscopy (FTIR) was used to observe chemical changes when nanomaterials are mixed with epoxy. It is shown that using ANPs at a concentration close to 2.0 wt.% can reduce the off-axis stiffness by ~30% and increase the off-axis stress-relaxation of CFRP by ~10%. Using NF-MWCNTs, it is shown that when incorporating 1.5 wt. % NF-MWCNTs, the stiffness decreases by ~60% and the off-axis stress relaxation of CFRP increases by ~12%. Finally, using F-MWCNTs, it is shown that the initial modulus of the CFRP composite decreases by ~25% and the relaxation increases by ~10% over a period of 1800 seconds.

Table of Contents

List of Figures

List of Tables

CHAPTER 1 INTRODUCTION

Deployable structures are commonly utilized in aerospace applications because of their ability to fold into a small geometry during stowage and completely expand into their service configuration when required. Sputnik 1, the first satellite released on October 4, 1957, was the first structure with deployable composites to be used for space applications (Tiber, 2002). Since then, there has been a tremendous amount of research performed to develop lightweight, stiff deployable structures. There are a variety of applications for deployable aerospace structures such as use in antennas, solar arrays, and structural booms. However, these applications typically require an external mechanism to allow deployment to occur. Not only does this increase weight on the system, but adds complexity to the design. As a possible solution towards the need for an external mechanism, it has been proposed to use strain energy driven deployments.

Strain energy driven deployable structures are commonly composed of thin laminates made of glass and/or carbon fibers. They are able to fold elastically and deploy through the release of the stored strain energy. Their low weight, ability to fold elasticity into small radii, and low-mass-to-stiffness ratio are reasons that strain energy deployable structures are beneficial in the aerospace field.

1.1 Challenges in Deployable Composites

There have been problems noted in the use of deployable composites. In 2003, the European Space Agency launched the Mars Express Mission. Onboard was the Mars Advanced Radar for Subsurface and Ionosphere Sounding (MARSIS), which was composed of three thin-walled booms. In 2004, it was discovered that the FEA model

underestimated the deployment dynamics of the hinge (Mobren et al., 2009). The hinge that was tested in the laboratory, prior to launch of the satellite, had undergone multiple thermal cycles and stowed for a period of time in its stowed configuration– allowing relaxation to occur and a reduction in torque which allowed for a laboratory optimal deployment speed. However, the hinge used in the satellite did not undergo the same testing and as such, the matrix did not relax, causing the hinge to have much higher deployment dynamics than anticipated (Brinkmeyer et al., 2015). In the final report, viscoelasticity was noted as one of the root causes of the incorrect behavior.

This ultimately raises the question as to how to control the deployment dynamics in strain energy deployable composites, such as a tape spring or hinge. For a strain energy deployable structure to work efficiently, it needs to have sufficient deployment forces in order to deploy; however, these forces cannot be too high as there is potential to cause damage to the structure. Viscoelasticity, ply angles, and number of plies have an effect on the behavior of the composite. Previous research performed at the Air Force Research Laboratories (AFRL) Composites Laboratory has shown it is possible for a tape spring to relax completely and not deploy (Peterson, 2015). To combat this problem, AFRL has designed an optimal laminate, known as a FlexLam tape spring. It is composed of unidirectional (UD) plies oriented at 0° from the tape axis sandwiched between plain weave (PW) plies oriented on the bias at 45° (Peterson, 2015).

While researchers continue to explore the optimization of deployment in tape springs through varying ply angles and thicknesses, there has been little research on engineering the viscoelastic properties of the carbon fiber reinforced polymer (CFRP) composite. The

purpose of this thesis is to focus on studying off-axis the viscoelastic properties of PW-CFRP and determine if nanomaterials will aid in controlling the behavior of the composite. The idea is to take advantage of the viscoelastic behavior of the matrix, knowing it is one of the controlling parameters of the off-axis behavior of CFRP composites.

It is well understood from literature that the addition of nanomaterials into a polymer system greatly changes its chemical, electrical, and mechanical behavior (Paul et al., 2008). Carbon nanotubes (CNTs) are used in a variety of applications because of their excellent mechanical, thermal, and electrical properties (Al-Saleh et al., 2011; Esawi et al., 2010). Alumina nanoparticles (ANPs) have been shown to increase the stiffness, fracture toughness, and glass-transition temperature of a polymer (Omrani, et al., 2009; Lim, et al., 2010). Furthermore, it has been shown that the behavior of the nanocomposite is dependent upon the concentration of the nanoparticles in the epoxy resin. For this reason, not only will different nanomaterials be studied and explored, but their respective concentration in the epoxy matrix will also be examined.

1.2 Thesis Purpose and Workflow

This thesis aims to explore how different nanomaterials and their respective concentrations affect elastic and viscoelastic (e.g. stress-relaxation) of CFRP composites. Moreover, nanocomposite behavior at the polymer base is studied and related to the CFRP composite. It is hypothesized that nanomaterials alter the viscoelastic behavior of the matrix, which changes the behavior of the CFRP composite. The ultimate goal of this research is to gain an understanding and characterize how different nanomaterials and their respective concentrations alter the behavior of fiber reinforced polymer composites.

Chapter 2 contains a review of polymers, linear viscoelasticity and its respective constitutive models pertaining to creep and stress relaxation. Research examining the use of nanomaterials in polymers is also discussed. This review will cover information on different nanomaterials such as multi-walled carbon nanotubes (MWCNTs) and alumina nanoparticles (ANPs). This chapter will conclude with an overview on polymer matrix composites.

Chapter 3 explains the experimental methods. Synthesis of the polymer nanocomposite, fabrication of the CFRP composite, and mechanical testing of the polymer nanocomposite and CFRP coupons are discussed. Furthermore, characterization methods used such as Dynamic Mechanical Analysis (DMA), and Fourier Transform Infared Analysis (FTIR) are reviewed.

Chapter 4 is a summary of the effect of alumina nanoparticles (ANPs), non-functionalized multi-walled carbon nanotubes (NF-MWCNTs), and COOH-functionalized MWCNTs (F-MWCNTs) on the elastic and viscoelastic (e.g. stress relaxation) behavior of CFRP. Using different weight concentrations of nanoparticles, observations from stress-relaxation experiments performed on plain-weave CFRP coupons are presented and used to understand the viscoelastic behavior of off-axis CFRP. Furthermore, microstructural analysis results from FTIR are presented and used to infer the macroscopic effect of ANPs, on the viscoelastic behavior of CFRP. Lastly, this chapter evaluates the behavior of the fiber reinforced polymer composites using analytical and rheological models.

Chapter 5 presents the conclusion of the experimental and analytical investigations. It also offers recommendations for future work in the field of viscoelastic behavior of CFRP composites incorporating nanomaterials.

CHAPTER 2 LITERATURE REVIEW

2.1 Introduction

Background information on viscoelasticity, nanocomposites and CFRP is reviewed in this chapter. The chapter begins with a review on viscoelasticity – namely stress relaxation and creep. The chapter then expands the topic towards understanding background information on nanomaterials and explains current research on the effect of nanomaterials in matrix materials. Furthermore, the chapter ends with a statement on current research on the effect of nanomaterials on FRP Composites.

2.2 Viscoelasticity

There is a subset of materials that exhibit time-dependent behavior, known as viscoelastic materials. Unlike elastic materials, which have a definite response to an applied stress, σ, viscoelastic materials show an increase in strain, $\varepsilon(t)$, as long as the load is sustained as shown in Figure 2.1a. This phenomenon is known as creep. The inverse of creep is stress relaxation. In stress relaxation, a sample is held in a constant state of strain and the stress drops as a function of time, as shown in Figure 2.1b.

Figure 2.1 Time-Dependent Behavior of Viscoelastic Materials

Two parameters are used to describe creep and stress relaxation behavior of a viscoelastic material (Meyers, 2009). The creep compliance, *J(t)*, is used to describe a specimen in a creep test, in which the specimen has a constant stress, σ_0, applied and strain is measured:

$$J(t) = \frac{\varepsilon(t)}{\sigma_0} \tag{2.1}$$

Conversely, relaxation modulus, *E(t)*, is used to describe the specimen during a stress relaxation test, in which the specimen is held in a constant state of deformation and the stress as a function of time is measured:

$$E(t) = \frac{\sigma(t)}{\varepsilon_0} \tag{2.2}$$

2.2.1 Constitutive Rheological Models

There are many models available to describe the behavior of viscoelastic materials. They are most commonly described by a spring and a dashpot. Equation 2.3 describes the elastic behavior of a spring. *E*, in this instance, is represented by the stiffness of the spring, and is also known as the modulus of a material. It is an inherent material property. As such, there is a definite response noted in stress, σ, when strain, ε, is applied:

$$\sigma = E\varepsilon \tag{2.3}$$

A dashpot is commonly used to describe the viscosity of the system. A dashpot is a system in which a cylinder is filled with a Newtonian fluid. Equation 2.4 describes this behavior where η is the Newtonian viscosity and $\frac{d\epsilon}{dt}$ is the change of strain with respect to time, *t*:

$$\sigma = \eta \frac{d\epsilon}{dt} \tag{2.4}$$

As its name suggests, viscoelasticity is a combination of both elastic behavior and viscous behavior. As such, there are models that use the spring (elastic part) and dashpot (viscous part) to describe the time-dependent behavior.

The Maxwell Model, shown in Figure 2.2, is a spring and dashpot connected in series. Equation 2.5 is the constitutive equation of the Maxwell model. In the Maxwell model, the system will first respond to the elastic portion as represented by a spring. Furthermore, the elastic portion will completely relax when the load is released. However, the viscous portion response gradually grows with time:

$$\frac{d\varepsilon}{dt} = \frac{1}{E}\frac{d\sigma}{dt} + \frac{\sigma}{\eta} \tag{2.5}$$

Integrating with respect to time:

$$\varepsilon(t) = \frac{\sigma}{E} + t\frac{\sigma}{\eta} \tag{2.6}$$

If strain is held constant and the equation is integrated, Equation 2.7 is the result:

$$\sigma(t) = E\varepsilon_0 e^{-t\left(\frac{E}{\eta}\right)} \tag{2.7}$$

As is true for most polymers, this model, upon integration, predicts that stress relaxation occurs exponentially. The term η/E is defined as the relaxation time, τ. However, it is important to note that this model does not accurately predict creep because it models strain as a linear function with time as seen in Equation 2.6.

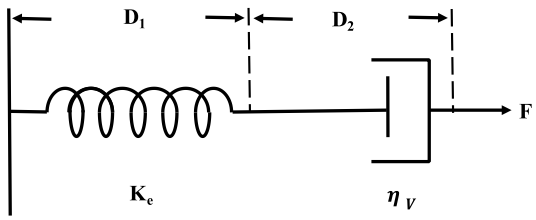

Figure 2.2: Maxwell Model

The Kelvin-Voigt model is a dashpot and spring connected in parallel, as seen in Figure 2.3 and represented by Equation 2.8. Since the dashpot and spring are connected in parallel, the strain across both elements is equivalent:

$$\sigma = E\varepsilon + \eta\frac{d\varepsilon}{dt} \tag{2.8}$$

Integrating and holding stress constant gives the following equation:

$$\varepsilon(t) = \frac{\sigma_0}{E}\left[1 - e^{-t\left(\frac{E}{\eta}\right)}\right] \tag{2.9}$$

In this instance, the term η/E is defined as the retardation time, τ.

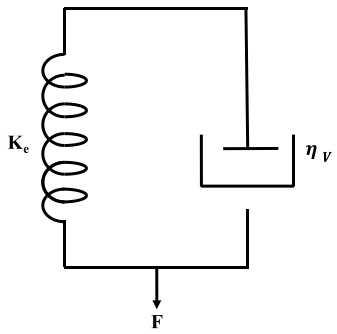

Figure 2.3: Kelvin-Voigt Model

The equations presented in Equation 2.1 and 2.2 can be used to derive the creep compliance, *J(t)*, and relaxation modulus, *E(t):*

$$J(t) = J_0\left[1 - e^{-\frac{t}{\tau}}\right], \text{ and} \tag{2.10}$$

$$E(t) = E_0 e^{-\frac{t}{\tau}} \tag{2.11}$$

While the Maxwell model is a reasonable representation of stress relaxation, it is inadequate to describe creep. On the other hand, while the Kelvin-Voigt model may adequately show the time-dependent response, it does not show the instantaneous response that is observed in most samples. The Maxwell-Weichart model, also known as the Generalized Maxwell model, consists of several Maxwell elements in parallel. Figure 2.4 is a representative element of the Generalized Maxwell equation. Since the elements are in

parallel with each other, this means that relaxation occurs over a period of time, instead of in a single element of time.

$$\sigma(t) = E_1\varepsilon_0 e^{-t\left(\frac{E_1}{\eta_1}\right)} + E_2\varepsilon_0 e^{-t\left(\frac{E_2}{\eta_2}\right)} + E_n\varepsilon_0 e^{-t\left(\frac{E_n}{\eta_n}\right)} + E_{eq}\varepsilon_0 \quad (2.12)$$

Figure 2.4: Generalized Maxwell Model

The Prony Series, seen in Equation 2.13, is a series of Maxwell models in parallel. The Prony Series is commonly used to describe the relaxation behavior of a material:

$$\ddot{E}_m(t) = E_{m0}\left(1 - \sum_{k=1}^{N} k_k(1 - e^{-\frac{t}{\tau_k}})\right), \quad (2.13)$$

Where k_k and τ_k are the Prony series coefficients, N is the number of series terms, and E_{m0} is the initial elastic modulus.

2.2.2 Dynamic Mechanical Properties

The viscoelastic properties of a material are often tested in a dynamic fashion, meaning the stress is applied sinusoidally, as seen in Figure 2.5 (Meyers et al., 2011). A viscoelastic material will exhibit delayed viscoelastic strain (time-dependent) when there is applied

stress on the system because its behavior derives from both viscous and elastic properties. In a viscous material, it will resist strain linearly with time when stress is applied.

The material is subjected to an oscillatory strain with frequency ω. Strain and stress are expressed as:

$$\epsilon = \epsilon_0 \sin(\omega t), \text{ and} \tag{2.14}$$

$$\sigma = \sigma_0 \sin(\omega t + \delta) \tag{2.15}$$

in which δ is the phase angle or phase lag between stress and strain due to the viscoelastic nature of the material. E′, the tensile storage modulus, and E″, the tensile loss modulus, are defined as:

$$E' = \left(\frac{\sigma_0}{\epsilon}\right) \cos(\delta), \text{ and} \tag{2.16}$$

$$E'' = \left(\frac{\sigma_0}{\epsilon}\right) \sin(\delta) \tag{2.17}$$

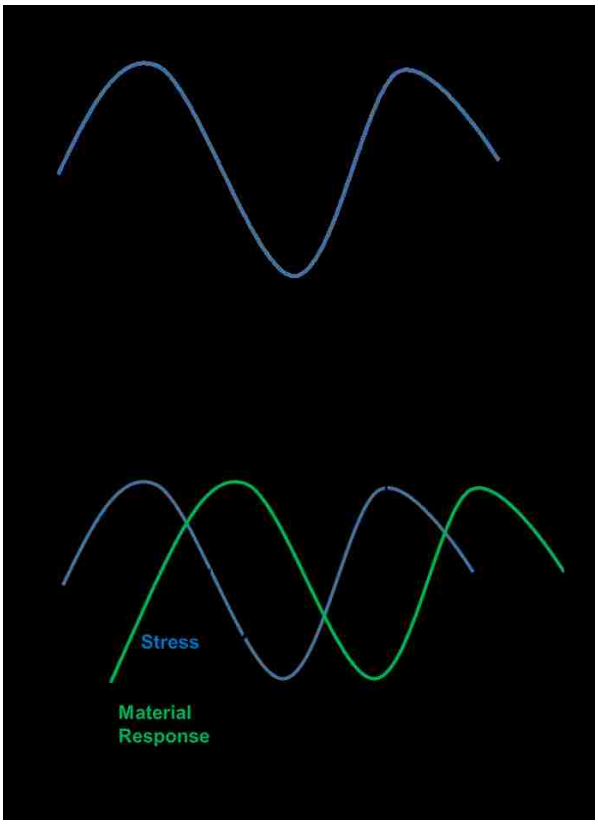

Figure 2.5: Sample Response after subjected to Oscillatory Force

The storage modulus and loss modulus can be explained by the dropping of a ball. When a ball is dropped and bounces, it is divided into two parts. The first part is the recovered part, or how high it bounced, and is described by E′. The energy loss in internal motion is E′′ as shown in Figure 2.6 (Menard, 2008).

Using complex variables, the modulus can be calculated as follows:

$$E = E' + iE'' \tag{2.18}$$

where i is the imaginary number $\sqrt{-1}$.

The loss tangent, tan δ, is defined as the ratio of the loss modulus to the storage modulus:

$$\tan \delta = \frac{E''}{E'} \tag{2.19}$$

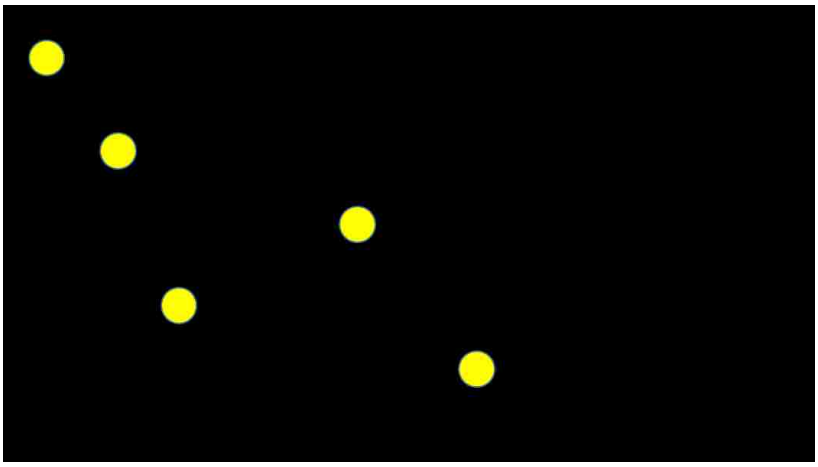

Figure 2.6: Energy loss from Ball Dropping (Menard, 2008)

2.2.3 Time-Temperature Superposition Principle

A polymer's behavior is largely dependent upon its temperature. Figure 2.7 demonstrates the different regions a polymer may experience under increasing temperature. As shown in Figure 2.7, in Region 1, under low temperature, a polymer is stiff and glassy. In Region 2, as the temperature increases, the modulus drops and the polymer begins to soften. Region 3 is known as the rubbery plateau and the material may behave in two different ways. If it is a crosslinked material, it will follow the dotted line and its modulus will remain constant. However, if it is linear, the modulus will drop off slowly. Region 4 is known as the rubbery flow region. And finally, Region 5 is known as the viscous flow region.

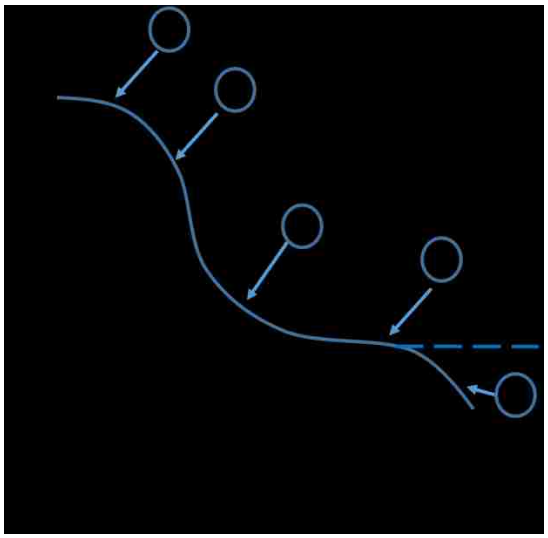

Figure 2.7: Temperature Dependence of a Polymer

As shown in Figure 2.7, polymers are temperature dependent. If a polymer is held at a constant load, the strain will continue to increase over time. Because of this, the time-temperature superposition principle (TTSP) is frequently used to determine the temperature dependence of a polymer or to extrapolate long-term data of a polymer at unknown times or frequencies (Gurp et al., 1998). Equation 2.20 is representative of this theory. The change in temperature from T to T_0 is equivalent to multiplying the time scale by a constant factor a_T which is only a function of the two temperatures T and T_0.

$$E(t,T) = E(a_T t, T_0) \tag{2.20}$$

Figure 2.8 is a pictorial diagram depicting the underlying basis of TTSP and generating master curves. It is important to note that the use of TTSP requires the assumption of thermologically simple behavior. This diagram shows the representative curves that would be generated under a stress relaxation experiment at three different temperatures, T_1-T_3. Figure 2.8(a) shows the typical material behavior generated at various temperatures and

(b) shows is representative of the final master curve after shifting the individual curves horizontally. The master curve of E′ versus its reduced time, t′, is generated by shifting E′ horizontally along the log scale of time. The horizontal shift factor, $a_{T_0}(T)$ is defined by Equation 2.21.

$$log a_{T0}(T, T_0') = \log a_{T0}(T, T_0) - \log a_T(T, T_0) \quad (2.21)$$

Figure 2.8 also shows that when the glass transition temperature, T_g, is chosen as the reference temperature then curves that are above T_g are shifted to the right and curves below the T_g are shifted to the left.

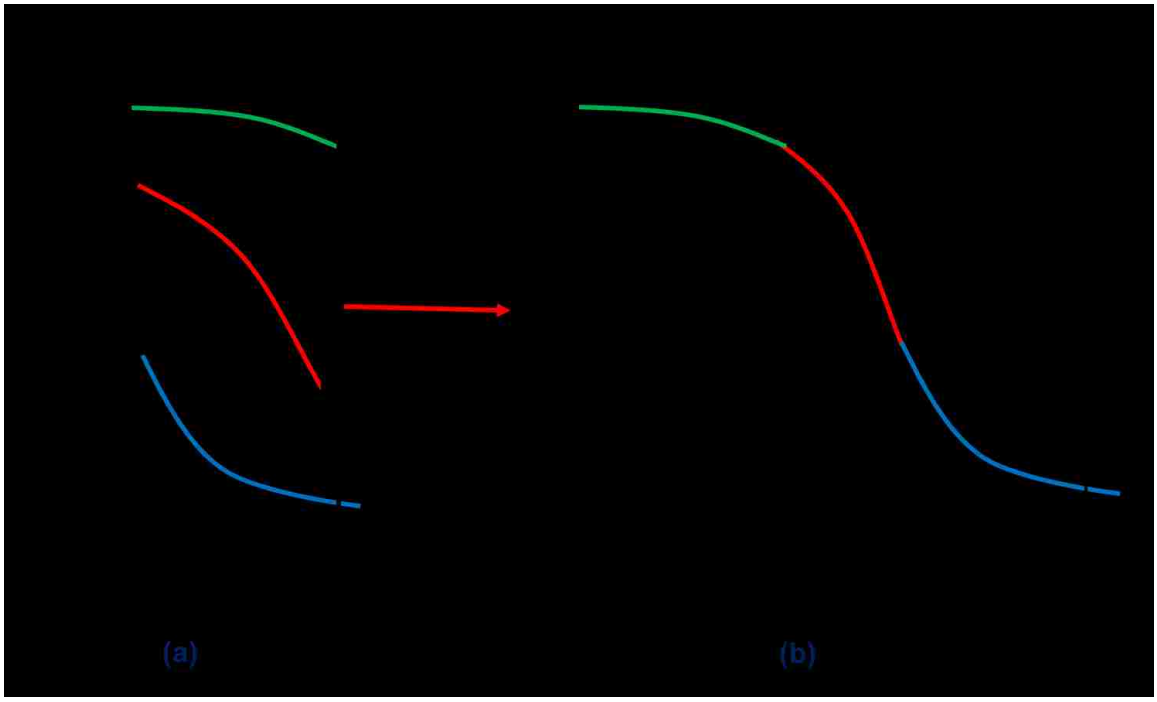

Figure 2.8 Time-Temperature Superposition

It was observed that there is a relationship between shift factor and temperature, and from this, the Arrhenius relationship was developed and is expressed below (Arridge, 1975).

$$a_T(T) = exp\left[\frac{E_a}{R}\left(\frac{1}{T} - \frac{1}{T_0}\right)\right] \quad (2.22)$$

where E_a is the activation energy for flow, T is the temperature, T_0 is reference temperature, and R is gas constant. This equation is deemed to be effective if a plot of the logarithm of the determined shift factor (a_T) vs the reciprocal absolute temperature produces a straight line. While this equation is primarily for samples above their T_g, it has also been shown to fit data for linear polymers in their plateau and terminal zones (Dealy et al., 2009).

The second model used to describe TTSP behavior is the Williams-Landel-Ferry (WLF) equation (Williams et al., 1955). It is an empirical equation often associated with time-temperature superposition for temperatures that are closer to T_g. The WLF equation is shown in Equation 2.23, where T is the temperature, T_r is the reference temperature, and C_1 and C_2 are constants to fit the shift factor, a_T.

$$\log(a_T) = \frac{-C_1(T-T_r)}{C_2+(T-T_r)} \quad (2.23)$$

TTSP is especially useful because it allows long-term prediction of a thermorheologically simple material in a relatively short time period.

2.3 Fiber Reinforced Polymer (FRP) Composites

FRP composites are beneficial in several applications because of their highly desirable mechanical and thermal properties. Their low weight, corrosion resistance, and high fatigue endurance limits make them ideal candidates for aerospace applications, the automobile industry, and infrastructure applications (Oskouei et al., 2010; Soliman et al., 2012; Kar et al., 2008). Recently, the use of CFRP has become of interest in strain-energy deployable structures for aerospace applications (Brinkmeyer et al., 2015). The Air Force Research Laboratory (AFRL) Space Vehicles Directorate has developed a tape spring, a type of a deployable structure, which utilizes the stored strain energy of the structure to self-deploy, therefore eliminating the need for external energy sources (Footdale et al., 2014; Footdale et al., 2011). Unlike a Storage Tubular Extendable Member (STEM) boom, a tape spring, due to its laminate design, is stable when it is in a rolled position and does not need external containment.

Figure 2.9: FlexLam Tape Spring

2.3.1 Lifecycle of Deployable Aerospace Structure

A deployable structure will undergo different phases in its lifetime, as seen in Figure 2.10.

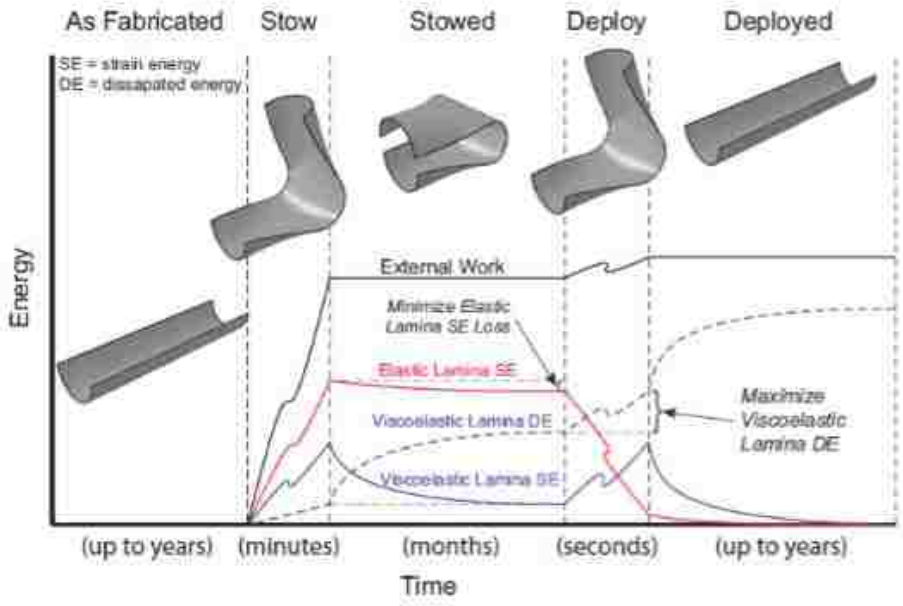

Figure 2.10: Lifecycle of a typical FlexLam Deployable Structure (Peterson, 2015)

A composite laminate is first fabricated and is stress free until it is placed in its designed stowed configuration for a period of days to years. The act of stowing places external work on the system relatively quickly and it is subjected to large strains. During this stowage time, the behavior of the laminate is dominated by the elastic properties from the carbon fibers, but also the viscoelastic properties from the matrix. As discussed earlier, because of the large strains that the structure is undergoing, the matrix experiences stress-relaxation, and the strain energy dissipate over the period of stowage. Finally, after an indefinite amount of time, the structure will deploy. The elastic lamina will use the stored strain energy to overcome the external forces, but is damped by the viscoelastic energy that

dissipated during stowage. The challenge is to engineer the viscoelastic energy loss in off-axis layer of tape spring so as to lower the deployment energy of the system.

2.3.2 Development of FlexLam Tape Spring

One of the critical aspects of controlling strain-energy in a deployable structure is understanding the time-dependent viscoelastic effects, especially during stowage. There have been reports of undesirable time-dependent viscoelastic effects taking place during stowage or deployment (Iqbal, et al., 2009). These reports have had extreme outcomes. For instance, work done at AFRL has shown that if too much relaxation occurs, the tape spring may not deploy. On the other hand, it has also been shown that if there is not enough relaxation, and dependent on the geometry of the laminate, the deployment energy is too high, potentially causing damage to the system. For this reason, the geometry of the laminate is critical when trying to define an optimal tape spring. As such, AFRL has developed an optimal laminate known as the FlexLam. It is a balanced and symmetric laminate composed of three layers. Layers 1 and 3 are unidirectional (UD) plies orientated at 0° between plain weave (PW) plies oriented on bias at 45°. The UD layers provide the required structural properties such as high axial stiffness. However, they have low transverse bending and shear stiffness which makes them difficult to fold without failure. Incorporating the PW layers in the middle of the UD plies at 45° adds shear stiffness and local bending stiffness to the laminate. When it is in its rolled stowage configuration, the PW ply is loaded in shear, which highly strains the matrix. Because of this, the behavior of this layer is largely dependent on the matrix properties. If we can exploit the behavior of the matrix, such as inducing a larger amount of stress relaxation in this layer, then it may be possible to control or engineer the behavior of the composite.

2.4 Nanomaterials

2.4.1 Nanomaterials in Polymer Matrix

It has been shown that incorporating nanomaterials in a polymer matrix can alter the viscoelastic properties. For instance, Skandani et al. studied the effect of surface grown ZnO nano rods on the time dependent behavior of composites (Skandani et al., 2014). Using a DMA, flexural creep tests were performed on neat carbon fiber, ZnO film sputtered on carbon fiber, and ZnO-grown nano rods on carbon fibers. It was shown that in comparison to the neat sample, ZnO-sputtered and ZnO-grown samples had a 14% and 23% reduction in creep compliance, respectively. Furthermore, the relaxation modulus was shown to increase in comparison to the neat carbon fiber sample. It was concluded that ZnO nano rods reduce the creep compliance because they act as obstacles to slow the rearrangement and slippage of polymeric chains. Further research has confirmed these findings (Guo et al., 2007; Skandani et al., 2012).

ANPs incorporated into a polymer matrix have been shown to have the ability to improve mechanical and viscoelastic properties such as the storage modulus, stiffness, impact energy, and failure strain (Omrani et al., 2009; Wetzel et al., 2003). Naous et al. incorporated 0 vol %, 0.5 vol%, 1.0 vol%, and 2.0 vol% ANPs into an epoxy matrix and studied the effect of ANPs on the dynamic mechanical, tensile, and fracture properties (Naous et al., 2006). It was shown that there was a trend in increasing T_g with increasing volume percentage of ANPs in the matrix. Tensile strength and fracture toughness also increased.

The effect of CNTs in a polymer matrix has been studied extensively (Thostenson et al., 2001; Guo et al., 2007). It has been shown that viscoelastic properties are dependent on even dispersion of CNTs in the matrix, as well as the concentration of nanoparticles. Montazeri et al. studied the viscoelastic and mechanical properties of incorporating different concentrations of MWCNTs in epoxy (Montazeri et al., 2011). Using weight percentages of 0.0 wt. %, 0.1 wt. %, 0.5 wt. %, 1.0 wt.%, and 2.0 wt. % MWCNTs, tensile and viscoelastic behavior were studied. It was found that as the nanotube value reached 1.0 wt. % and 2.0 wt.%, the storage modulus decreased. It is suggested that this is due to the increase in agglomeration of the CNTs as a higher weight concentration making the movement of chains easier. Interestingly, their research showed that T_g decreased as the concentration of CNTs increased, representing a loss of crosslinking. Guadagno et al. studied the effect of functionalization of MWCNTs on the thermo-mechanical and electrical properties in epoxy-nanocomposites (Guanagno et al., 2011). When 1.0 % non-functionalized MWCNTs are added, there was a 20% increase in storage modulus. In contrast, when using functionalized MWCNTs there is not a constant increasing pattern in modulus seen with increasing concentration nanotubes. Furthermore, when using functionalized MWCNTs, T_g was shown to decrease with increasing nanotube concentration. Functionalized MWCNTs are typically used to help create a uniform dispersion in the polymer matrix (Wu et al., 2007). There have been many studies on how to properly functionalize the MWCNTs. However, as the main purpose of this thesis is to study the relaxation behavior of nanocomposites, different methods for functionalizing nanotubes will not be discussed.

2.4.2 Viscoelasticity in FRP

FRP are utilized in many different industries such as aerospace, automotive, and infrastructure because of its highly desirable properties. Many of these applications require lifespans of at least 20 years and as such, it is important to study time-dependent properties of FRP. For most composites, the matrix is responsible for the viscoelastic behavior as carbon fibers show negligible viscoelastic behavior (Qiao et al., 2000). This time-dependent behavior could be detrimental for FRP structures that are used in load-bearing applications or as an effort to aid in structural rehabilitation (Sullivan, 1991). Oskouei et al. studied relaxation of FRP in prestressing (Oskouei et al, 2010). Their research utilized different test set-ups to simulate typical pre-stressing environments and showed that the relaxation behavior of FRP is a combination of many attributes such as fiber relaxation (in aramid and glass fibers), interface between matrix and fibers, potential tears in the fibers, and matrix relaxation. While viscoelastic behavior is dependent upon many elements such as laminate lay-up, stress level, and temperature, Ma et al. studied AS-4/PEEK [$\pm$45] composites as an attempt to understand and characterize the shear creep properties as a function of stress and temperature (Ma et al., 1997). Tuttle and Brinson performed key research on prediction of the long-term creep of composite laminates (Tuttle et al., 1986). Based on these studies, it is proposed that the matrix is the dominant and controlling factor in the viscoelastic deformation found in FRP composites. As discussed below, it has been found that nanomaterials can aid in enhancing the electrical, mechanical, thermal properties when incorporated in FRP. It is now critical to understand the time-dependent properties of FRP when nanomaterials are used in FRP.

2.4.3 FRP incorporating nanomaterials

Soliman et al. studied the on and off-axis tension behavior of CFRP incorporating pristine and functionalized MWCNTs at different loading contents (Soliman et al., 2012). It was found that in off-axis testing, the mechanical properties of the functionalized MWCNTs-composite increased. In similar research, Zhou et al. researched the improvements in FRP when using carbon nanofibers (CNFs) (Zhou et al., 2008). Their work first studied the effect of CNFs in epoxy. After determining the optimal weight percentage of CNFs in the epoxy (2 wt. %), they then used this loading content to fabricate the FRP. There was a 22% and 11% increase in the flexural and tensile strength of the FRP, respectively, when using 2 wt. % CNFs in the epoxy. Gojny et al. incorporated low weight fractions of DWCNT-NH_2 and carbon black (CB) into an epoxy matrix to be utilized in fabrication of GFRP (Gojny et al., 2005). An increase in tensile properties were not observed when nanomaterials were used in the matrix for GFRP because the fiber-reinforcement dominates the mechanical properties. However, the interlaminar shear strength did improve when both DWCNTs-NH_2 and CB were utilized in the matrix. Hussain et al. showed that incorporating nano- and micro-sized Al_2O_3 fillers in the epoxy matrix to be used for fabrication increased the mechanical properties of the FRP (Hussain et al., 1996). Further work has been done studying the influence of incorporating COOH-MWCNTs into CFRP for impact loading (Soliman et al., 2012). It was found that when 1.5 wt. % COOH-MWCNTs are incorporated into the matrix, the penetration energy of the CFRP composite increases and the damage size is smaller. Genedy et al. studied the impact of COOH-MWCNTs on the fatigue performance of GFRP. Through fatigue testing and microstructural analysis, it was shown by incorporating 0.5 wt. % and 1.0 wt. % MWCNT, the fatigue life of GFRP increased by 1143 % and 986 %, respectively (Genedy, et al.

2015). Borowski et al. studied the impact of COOH-functionalized MWCNTs on the fracture toughness of CFRP. Through their work, it was found that the fracture toughness of unidirectional CFRP increases by 25% when 0.5 wt. % MWCNTs were incorporated into the composite (Borowski, et al., 2015)

During the literature review, it was found that there were very few studies pertaining to studying the time-dependent properties of FRP incorporating nanomaterials. Glaskova-Kuzmina et al. performed a study on the creep characteristics of epoxy and CFRP incorporating 1.0 wt. % CNTs (Glaskova, T., et al. 2014). Neat and CNTs (1.0 wt. %) epoxy/CFRP specimens were fabricated and tested in three-point bending. It was found that there was a reduction in the creep compliance for both the epoxy and CFRP, most notably seen when under higher stress level, leading to the presumption that incorporating CNTs in a matrix and CFRP improves the time-dependent properties in comparison to composite structures sans nanomaterials.

CHAPTER 3 EXPERIMENTAL METHODS

This chapter explains the experimental methods used in the synthesis, fabrication, and testing of the polymer nanocomposites and CFRP. It begins with an introduction to the materials that were used in the research including the plain-weave carbon fibers, functionalized COOH-MWCNTs, non-functionalized MWCNTs, alumina-nanoparticles (ANPs), and the epoxy. It describes the mechanical and chemical testing that was performed on three specimens including dynamic mechanical analysis (DMA), Fourier Transform Infared Spectroscopy (FTIR), and CFRP tensile testing.

3.1 Materials

The nano-Al_2O_3 particles used in this study were supplied by Sigma Aldrich with an average particle size of less than 50 nm. The non-functionalized and functionalized MWCNTs were were provided by Cheap Tubes, Inc. Both the functionalized and non-functionalized MWCNTs have an outer dimension of 20-30 nm, an inner dimension of 5-10 nm, and a length of 10-30 μm. The resin used is a diluted liquid based on diglycidyl ether Bisphenol-A and the hardener is an aliphatic Amine, both supplied by US Composites, Inc. The resin to hardener mixing ratio is 2:1, the pot life is 30-5 minutes at 80° F, the set time is 5-6 hours, and the curing time is 24-48 hours at room temperature. Because of its long pot life and low viscosity, it is an ideal candidate for the hand lay-up technique used in composite fabrication. The tensile strength and tensile elongation for the epoxy are 65 MPa and 25%, respectively (Soliman et. al, 2012). The carbon fiber fabric used in fabrication was also supplied by US Composites. It is a FG-CARB5750, balanced plain bidirectional weave and has a 3K tow size and thickness of 254 μm. The tensile

strength of the carbon fibers is 4.48 and the tensile modulus is 231 GPa (Soliman et. al, 2012). Table 3.1 contains the weight concentrations used in the synthesis and fabrication of the polymer nanocomposites and CFRP. Note that wt. % represents nanomaterials weight relative to the weight of the epoxy.

Table 3.1: Specimens Prepared

Material	Wt. %
Neat	0.0
ANPs	1.0
ANPs	2.0
ANPs	3.0
COOH-Functionalized MWCNTs	0.5
COOH-Functionalized MWCNTs	1.0
COOH-Functionalized MWCNTs	1.5
Non-Functionalized MWCNTs	0.5
Non-Functionalized MWCNTs	1.0
Non-Functionalized MWCNTs	1.5

3.2 Material Preparation

3.2.1 Synthesis of Polymer Nanocomposite

The epoxy and nanomaterial was first synthesized before being cast as either polymer nanocomposite beams or fabricated for use in CFRP. First, the nanomaterial was added to the resin and the mixture was sonicated for 1 hour at 40° C. The purpose for sonication is to generate microbubbles to help improve the dispersion of the nanoparticles. Next, the nano-particle resin mixture was mechanically stirred for 2 hours at 80° C to ensure the chemical reaction between the nanomaterials and the resin chains. Once cooled, the hardener was added to the resin mixture, hand stirred for 10 minutes, and then was used in fabrication or to cast epoxy beams. The polymer-nanocomposite beams cured uncovered

at room temperature for 6 hours, then were covered with a weight placed on top for a further 42 hours at room temperature. Finally, after a total of 48 hours of curing at room temperature, the specimens were cured at 60° C for another 48 hours. Figure 3.1 depicts the process used in synthesis of the nanocomposite.

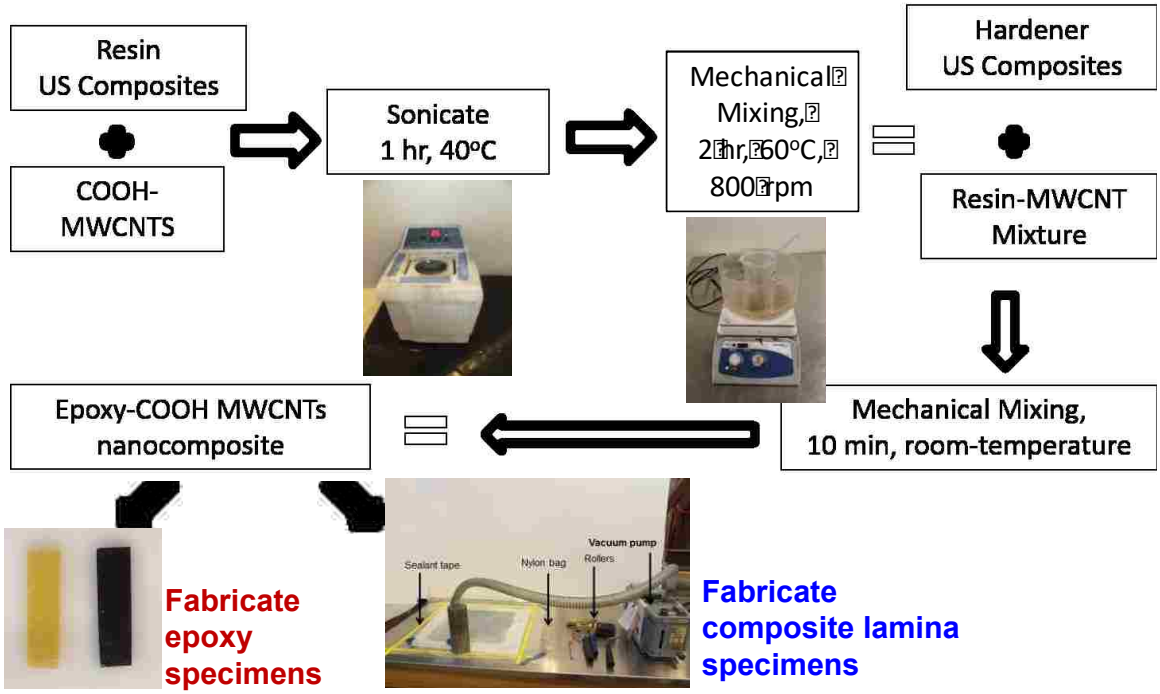

Figure 3.1: Synthesis of Polymer Nanocomposite

3.2.2 Fabrication of CFRP Composite

The hand-layup technique was used in the fabrication of the CFRP composite and was performed in accordance to ASTM D5687 standards (ASTM D5687/D5687M-95, 2015). Three fabric layers were used to fabricate the off-axis coupons. The procedure for creating the FRP composite is:

1. Attach non-porous release film over metallic plate
2. Place peel ply on top of release film
3. Distribute ¼ polymer nanocomposite mix on the peel ply
4. Place 1 layer of plain-weave carbon fiber on the matrix and using a roller, impregnate the fibers with the matrix
5. Repeat steps 3-4 until all layers have been placed and rolled
6. Place a second layer of peel ply on the carbon fibers
7. Place porous release film
8. Place breather ply layer
9. Place nylon bag on the top of the system
10. Place high-temperature sealant tape around the nylon bag and vacuum tube hose
11. Turn on pump for 24 hours

The non-porous release film is used to separate the composite from the plate. The peel ply layers were used to ease peeling of the composite after curing. The breather ply layer is used to absorb excess of the matrix. The vacuum pump had a pressure of $2.3*10^{-2}$ Torr and the fabricated specimen was held under vacuum pressure for 24 hours. The release films, peel plies, breather ply, nylon bag, and sealant tape were supplied by ACP

Composites, Inc. Figure 3.2 is a depiction of the hand-layup technique used. Figure 3.3 depicts a CFRP composite as fabricated under vacuum.

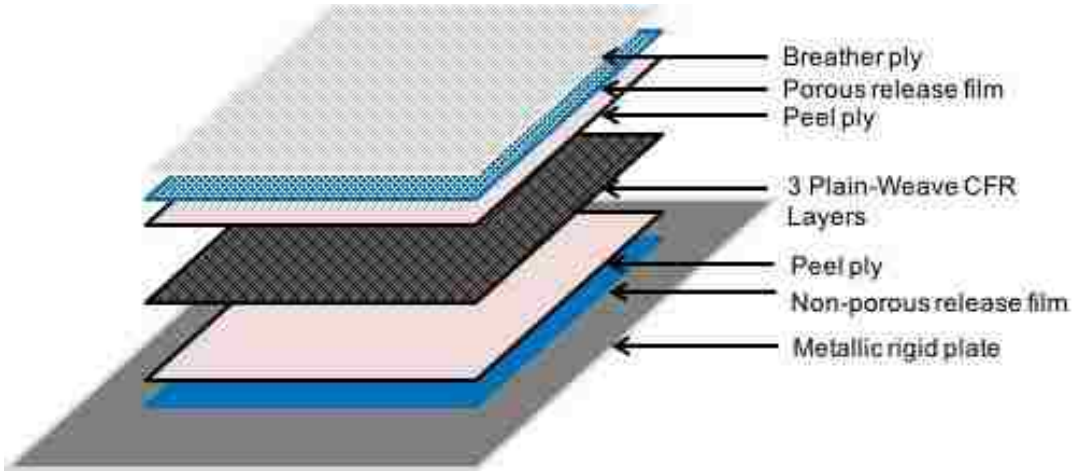

Figure 3.2: Fabrication of CFRP Composite (ASTM D5687/D5687M-95, 2015)

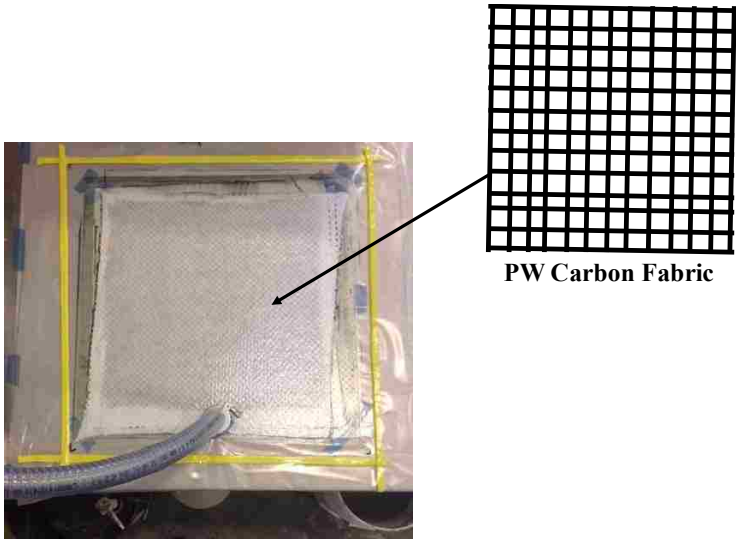

Figure 3.3: CFRP Composite under Vacuum Pressure

3.3 Dynamic Mechanical Analysis

Dynamic mechanical analysis (DMA) is a tool commonly used for material characterization. It works by applying an oscillatory force and then measuring the material's response to that force. In comparison to typical tensile testing, it measures the tendency to flow as well as the stiffness, which relates to viscosity and elasticity of the sample. As such, it has the ability to measure the viscoelastic properties of a material. The DMA Q800 by TA Instruments was used and is shown in the schematic below.

Figure 3.4: DMA Q800 Schematic (TA Instruments, 2010)

The primary outputs that were used in this analysis were relaxation modulus, time, tan δ, and temperature. Specimen geometry and choosing the correct clamp is key in accurate measurements. For this research, the film tension clamp was used and the load applied can be either static or dynamic.

Because there are very little standards pertaining to DMA testing, it is recommended to remain consistent through the testing. Stiffness and geometry are directly related to each other and is a key aspect to understand when preparing and running specimens. It is important to understand that both thick and thin samples can have the same stiffness because their modulus values are different. Similarly, a thick and thin sample can have the same modulus, but different stiffness's as seen in Figure 3.5.

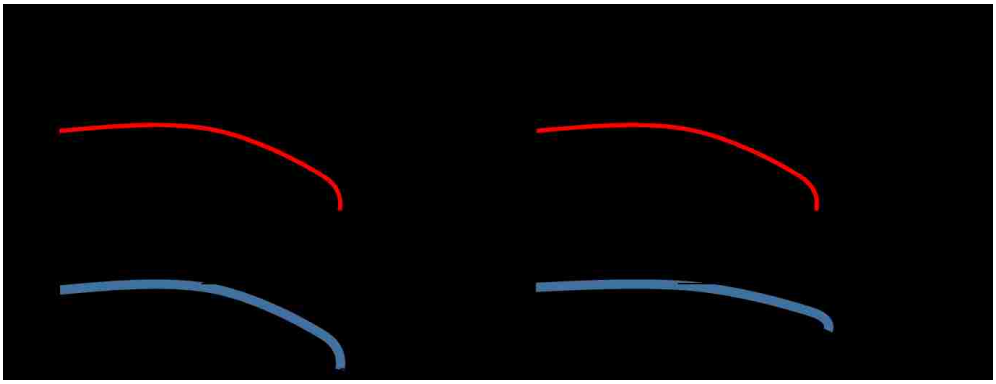

Figure 3.5: (a) Thick and thin samples can have the stiffness (b) Thick and thin samples that have the same modulus (TS-63, TA Instruments)

The geometry factor (GF) is defined by Equation 3.1 where L is the length of the specimen (mm) and A is the cross-sectional area (mm^2).

$$GF = \frac{L}{A} \tag{3.1}$$

The stiffness of the specimen is calculated by the following equation where KS is the stiffness (TS-63, TA Instruments)

$$KS = \frac{Modulus}{GF} \tag{3.2}$$

Figure 3.6 is a graphical representation of the relationship between stiffness and geometry factor. It is important to note that the measureable stiffness range of the instrument is between 100-10,000,000 N/m.

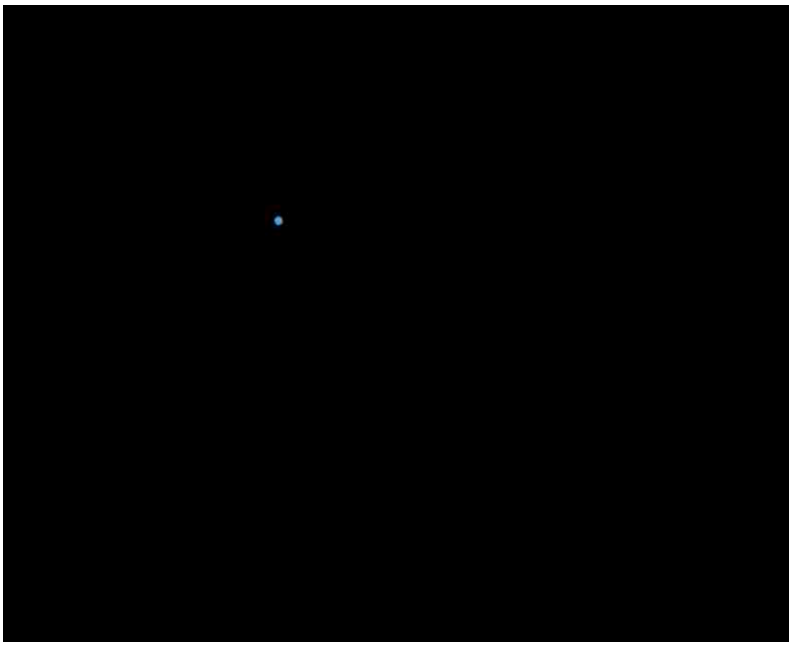

Figure 3.6: Graphical representation of relationship of GF and stiffness for tension film clamp (TA Instruments, 2015)

3.3.1 Sample Preparation

Samples were prepared for testing using the synthesis methodology described above. After curing, the polymer nanocomposites were cut into 30 mm x 5 mm x 1.25 mm beams using a Buehler-Isomet 4000 saw because it has high precision necessary to meet the geometry requirements of the DMA.

3.3.2 Determination of Linear Viscoelastic Region (LVR)

To properly describe the viscoelastic behavior, it is important to run experiments in a region where the properties observed are independent of the applied stress or strain. This region is called the linear viscoelastic region (LVR). There are two different techniques for determining the LVR. The first is monotonic creep and the second is by applying dynamic oscillation. To determine the LVR using the first method, a range of stresses is applied to the same material (TA Instruments, RS-23). Then, creep compliance is plotted for the material. If one stress does not overlap with the other stresses, this is indicative of it being outside of the LVR.

The second approach, using dynamic oscillation, uses the same frequency throughout the experiment, but increases the stress or strain applied. When the complex modulus or complex viscosity differs by more than 10% from the normalized constant plateau value, this indicates the sample is outside of the LVR (TA Instruments, RS-23).

To determine the LVR for this research, the second method was utilized using the strain-sweep experiment in the DMA. Using a constant frequency of 1 Hz, the modulus was recorded as the strain increased from 1 μm to 100 μm. After the experiment, the normalized storage modulus was plotted against the strain to determine the LVR.

3.3.3 Determination of Glass-Transition Temperature (T_g)

The glass-transition temperature (T_g) is one of the most critical characteristics of a polymer. The T_g is the region in which a material transforms from a brittle "glassy" state to a rubber-like state. While there are several methods that can be used to determine the glass-transition of a polymer, the most sensitive method is through DMA (TA Instruments, TS-64). There are three different parameters that can be used to determine the T_g and are shown in Figure 3.7:

- E' Onset: Occurs at the lowest temperature
- E'' Peak: Occurs at the middle temperature is related to the changes in the physical properties
- Tan Delta (δ) Peak: Occurs at the highest temperature and is most frequently used in literature

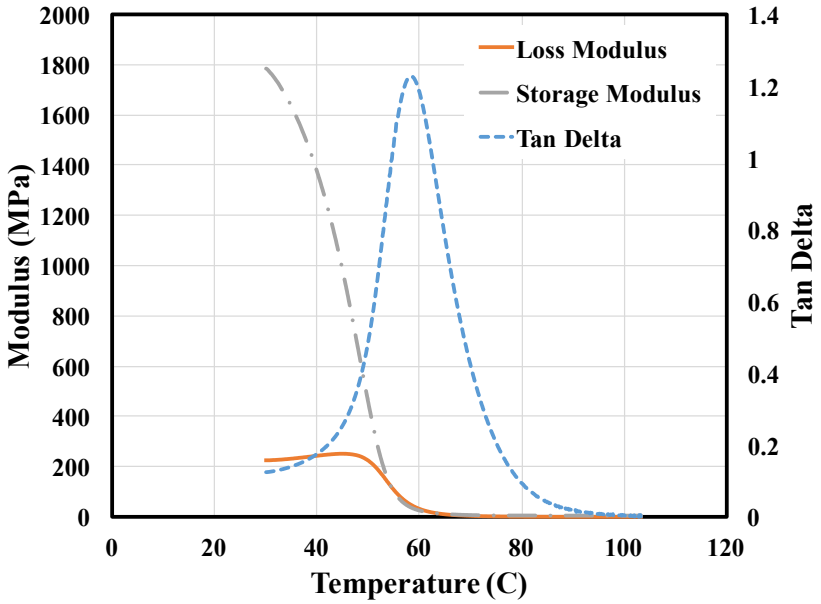

Figure 3.7: Glass Transition of Epoxy incorporating ANPs

The glass transition temperature was determined by increasing the temperature at a rate of 3 °C/min to 120 °C at a frequency of 1 Hz using the tension clamp. A ramp rate of 2 °C/min was chosen to ensure even heating of the specimen. The glass transition temperature was determined by the maximum value of tan δ.

Figure 3.8: Specimen in Tension in DMA

3.3.4 Stress Relaxation using Time-Temperature Superposition (TTSP)

Time-temperature superposition principle (TTSP) was used to extrapolate stress relaxation curves for the polymer nanocomposite specimens. As discussed earlier, TTSP states that the behavior of a polymer at a high temperature is equivalent to a longer amount of time at a lower temperature. Therefore, time and temperature can be interchanged. It is especially helpful when trying to predict the long-term behavior of a specimen at values that would typically take too long to test for (such as years) in a relatively short amount of time.

First, the strain rate and T_g of the specimen was determined. To determine the strain rate, the LVR needed to be determined. The T_g is critical to know because it is important to test a sample through its glass transition stage – for this reason, it is recommended to test 30 °C below the T_g (TA Instruments, TA-144A). Samples were held in the tension clamp with a preload force of 0.01 N and held constant at a strain of 0.05%. Samples were tested from 30 °C to 70 °C with a temperature increment of 5 °C. The isothermal soak time was 60 minutes and the relaxation time was 10 minutes.

Once the experiment finishes, the DMA outputs the relaxation modulus, time, tan delta, strain, and stiffness for each temperature. After exporting and transferring the raw data file, the first step is to normalize the data so that it is on the same time scale. After normalizing the data, it is necessary to convert both the time and the relaxation modulus to log scale. This can be seen in Figure 3.9(a). The next step is then to choose a reference temperature to shift all of the data to. For this specific example, a reference temperature of 30 °C was chosen. To perform "shifting," the curves must be superimposed on each other. This is accomplished by horizontally shifting the curves – adding a constant to each designated temperature's time.

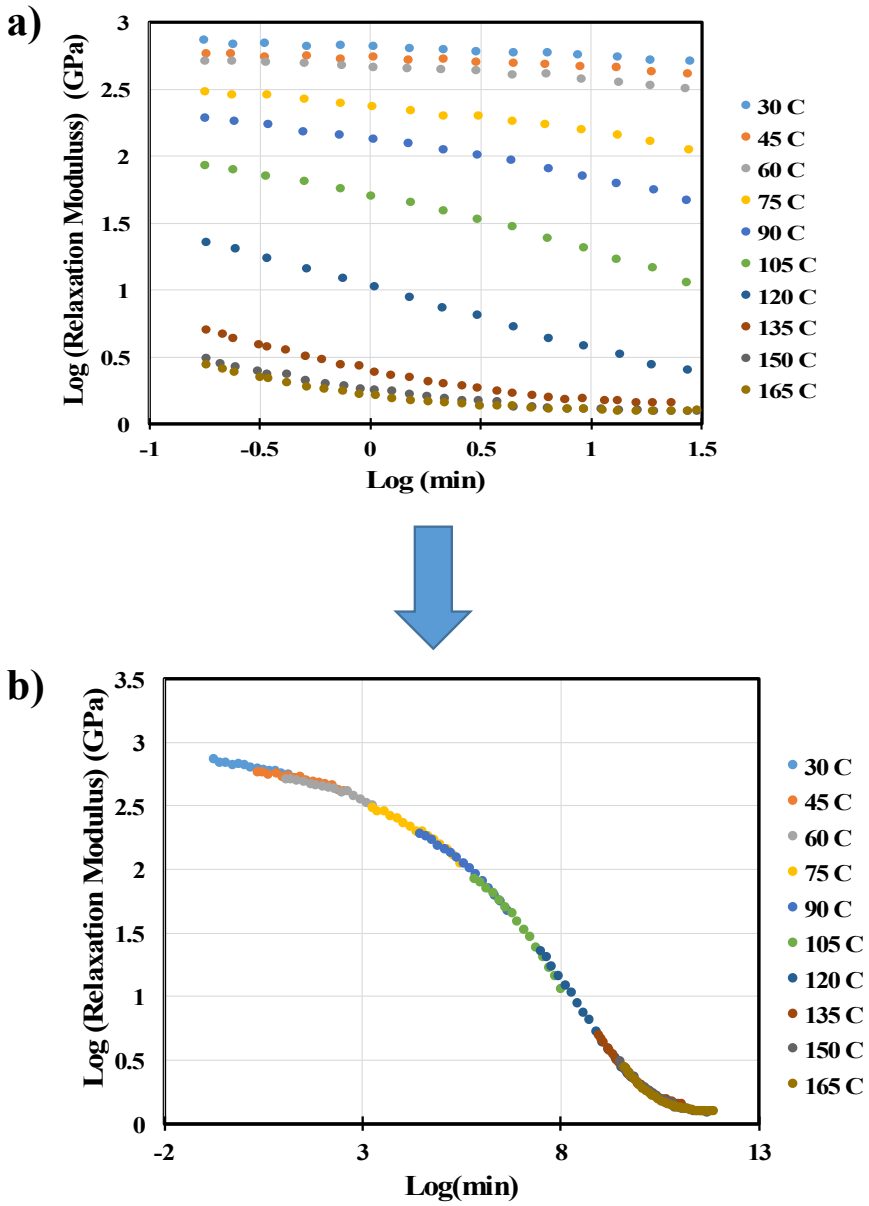

Figure 3.9: Stress Relaxation Behavior of 3501-6 Epoxy Resin (a) Non-shifted data (b) Shifted data (Yeong, et al, 1996)

3.4 Fourier Transform Infared Spectroscopy

Fourier transform infared spectroscopy (FTIR) was used to investigate if a chemical reaction had taken place between the nanomaterials (ANPs, functionalized-MWCNTs, non-functionalized MWCNTs) and the epoxy. To perform FTIR on the samples, they were cut to a dimension of 25 mm x 25 mm x 0.5 mm. 4000 scans were collected at a resolution of 4 cm^{-1} using a horizontal attenuated total reflectance (ATR) and a DiComp Crystal. The data was analyzed using a PerkinElmer FTIR with Universal ATR which were converted to absorbance using Kramers-Kronig equations (Griffiths, 2007). The key peaks that were observed for changes when looking at samples were the epoxide ring (~830 cm^{-1}), OH group (~3400 cm^{-1}), C=O stretch at 1735 cm^{-1}, and finally, the NH band of primary amines (1580-1650 cm^{-1}).

3.5 CFRP Testing

This section explains the processes used for prepping the coupons, determining the fiber volume section, and testing the coupons. CFRP coupons were cut from the large composite plates fabricated into a dimension of 25.4 mm x 203.2 mm. The grips at the top and bottom of the coupon were 25.4 mm as seen in Figure 3.10.

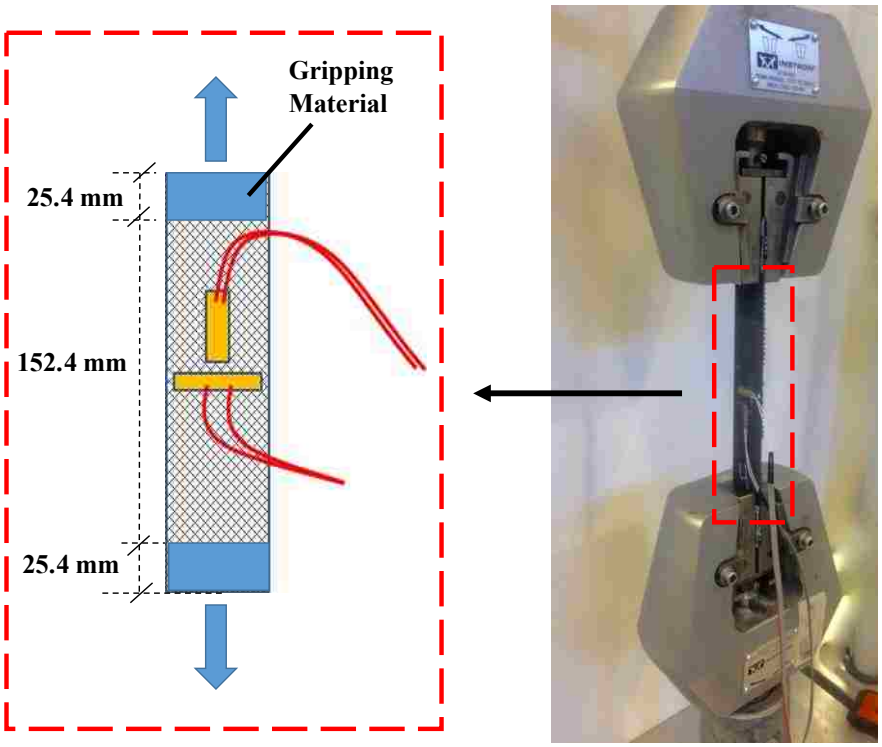

Figure 3.10: CFRP Test-Set Up

The strain gauges used were supplied by Omega Engineering, Inc. Omega KFH-10-120-C1-11L33R were used and had a gauge length of 10 mm and a resistance of 120Ω. Strain gauges were applied in the center of the coupon in the axial and transverse directions.

The off-axis tension test followed ASTM standards D3518/D318M-13 (ASTM D3518/D318M-13, 2013.) This test examines the in-plane shear behavior of the CFRP composites. To compare the effect of different concentrations of nanomaterials in the CFRP in stress relaxation, all specimens were tested in tension under stress-relaxation using a MTS® Bionix servo hydraulic system, which has a load capacity of 25 kN. In accordance with ASTM D3039, five specimens were examined in each test (ASTM D3039/D3039M-14, 2014). Two strain gauges were placed on each specimen to measure both the axial and transverse strain. The specimens were loaded in a displacement control

mode with a loading rate of 1 mm/min up to a displacement of 2.286 mm. Once specimens reached the desired displacement, they were held for 30 minutes. For each coupon, the stress-strain relationship was obtained and shear chord modulus G_{12} were obtained.

Shear stress was calculated using Equation 3.3 seen below where P is the force and A is the cross-sectional area of the composite:

$$\tau_{12} = \frac{P}{2A} \tag{3.3}$$

The shear strain was calculated as:

$$\gamma_{12} = \epsilon_x - \epsilon_y \tag{3.4}$$

The shear chord modulus was calculated over a range of 4000 $\pm$200 με starting with a lower strain range value of 1500 to 2500 με using Equation 3.5:

$$G_{12}^{chord} = \frac{\Delta\tau_{12}}{\Delta\gamma_{12}} \tag{3.5}$$

where G_{12}^{chord} is the shear chord modulus of elasticity, $\Delta\tau_{12}$ is the difference in applied shear stress between the two shear strain points, and $\Delta\gamma_{12}$ is the difference in shear strain between the two shear stress points.

3.6 Determination of Fiber Volume Fraction

The fiber volume fraction, V_f, was determined for all CFRP specimens to use for composite analysis calculations. V_f was determined using the acid digestion method per ASTM D3171 Procedure A – matrix digestion using nitric acid (ASTM D3171/15, 2015).

In this procedure, the composite is placed in an acidic solution and heated as an effort to break down the matrix and leave only the fibers. V_f can be calculated:

$$V_f = \frac{M_f}{M_d}\frac{\rho_c}{\rho_f}, \tag{3.6}$$

Where M_f is the final fiber mass, M_d is the dry mass, ρ_c is the density of the composite, and finally, ρ_f is the manufacturer specified density.

Figure 3.11: Determination of Fiber Volume Fraction

CHAPTER 4 RESULTS

4.1. Introduction

This chapter will overview the experimental work done on CFRP incorporating ANPs, NF-MWCNTs, and F-MWCNTs. DMA results and FTIR results will also be discussed.

4.2 Off-axis Stress Relaxation of CFRP Including Alumina Nanoparticles

Modeling of epoxy-ANPs nanocomposite

The rule of mixtures model is a commonly used model to predict Young's modulus of polymers reinforced with micro particles or fibers. However, the rule of mixtures does not take into account fiber orientation and fiber-matrix interaction (Omidi et al., 2010; Cox, 1952). The modified rule of mixtures for discontinuous reinforcement is also a commonly used model because it takes into account the significance of bond of the fiber/particle reinforcement with the matrix. It is typically found that as the nanomaterial content increases, the mechanical properties such as modulus and stiffness of the polymer increase (Bortz et al., 2011; Esawi et al., 2010). Using the modified rule of mixtures for discontinuous reinforcement in Equation 4.1 the modulus of the composite can be calculated (Kuo et al., 2005).

$$E_c = \eta E_p V_p + E_m V_m \tag{4.1}$$

where the modulus of the composite, reinforcement, and matrix are represented by E_C, E_p, and E_m and the volume fraction of the nanomaterials in the epoxy represented by V_r and V_m respectively. The strengthening coefficient, η, is assumed to be ~0.1 for nanoparticles with an aspect ratio of ~1 (Kuo et al., 2005). E_m can be determined from DMA testing of neat

matrix and E_p is obtained from literature or manufacturing specifications. Furthermore, the Halpin-Tsai equation was also used to predict the modulus of elasticity of the epoxy-nanocomposite as described in Equation 4.2.

$$E_c = E_m * \left(\frac{1 + \xi \eta V_p}{1 - \eta V_p} \right) \tag{4.2}$$

Where:

$$\eta = \frac{\frac{E_f}{E_m} - 1}{\frac{E_f}{E_m} + \xi} \tag{4.3}$$

A value of 2 is assumed for the constant (ξ) when spherical reinforcement is used (Naous et al., 2006).

Results and discussion

Off-axis median stress-strain curves of carbon fiber reinforced polymer (CFRP) incorporating varying content of alumina nanoparticles (ANPs) are presented in Figure 4.1 and the mean results of the shear modulus are presented in Table 4.1. The mean shear chord modulus for neat CFRP was found to be 1766 MPa. When 1.0 wt.% ANPs are incorporated in the matrix prior to fabrication, the modulus decreases slightly to 1719 MPa, which is a 2.6% decrease over the neat CFRP. As the concentration of ANPs increased to 2.0 and 3.0 wt.%, the mean shear chord modulus significantly decreased to 1262 MPa and 1243 MPa respectively. This is a 29% and 30% reduction from neat CFRP shear modulus. It should be noted that while no significant statistical difference was found between the 2.0 and 3.0 wt.% ANPs, a significant difference was found when comparing shear modulus of neat CFRP and CFRP incorporating 2.0 wt.% ANPs. It is evident that incorporating 2.0 wt.%

ANPs in epoxy prior to CFRP fabrication can significantly reduce the off-axis stiffness and thus off-axis strain energy by ~30%.

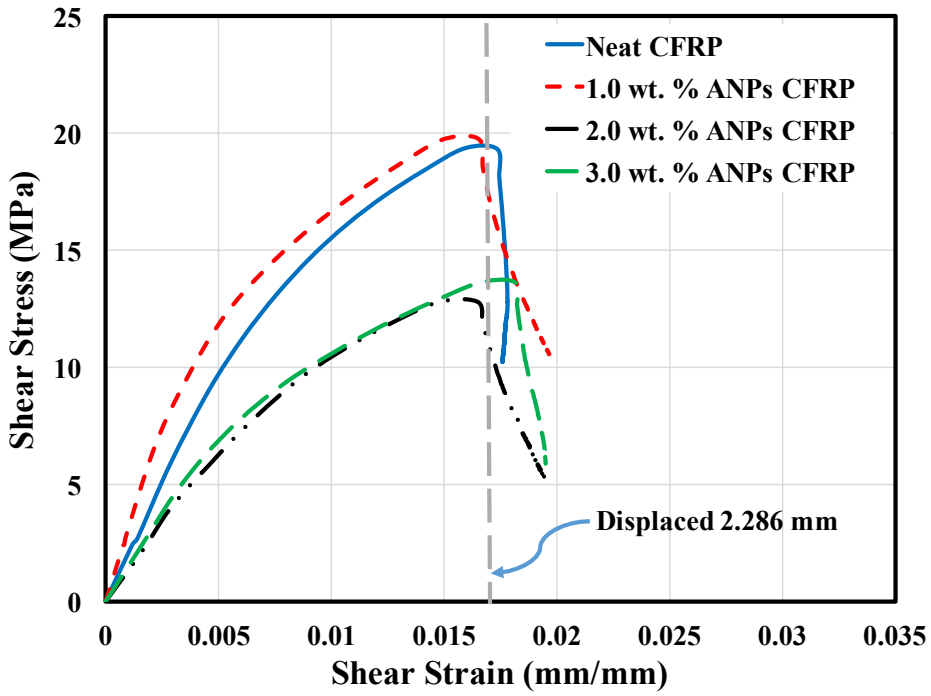

Figure 4.1: Stress-Strain relationship for CFRP coupons with varying levels of ANP (Curves shown represent represent median out of 5 tested coupons).

Table 4.1: Mean off-axis shear modulus (± standard deviation) of CFRP coupons incorporating ANPs.

CFRP type	G_{12} (MPa)
Neat	1766±88.4
1.0 wt.% ANPs	1733±98.5
2.0 wt.% ANPs	1261±107.8
3.0 wt.% ANPs	1243±103.8

The initial tangent modulus (E_0) and stress-relaxation of CFRP incorporating ANPs was also determined. The mean initial tangent modulus of neat CFRP coupons was found to be 2408 MPa and 1.0 wt.% ANPs had an initial mean relaxation modulus of 2683 MPa, which is a 4.6% increase over the neat CFRP. Similar to the analysis of shear chord-modulus, E_0 for both 2.0 and 3.0 wt.% ANPs was found to be about 34% and 38%,

respectively, lower than E_0 of neat CFRP. This trend continues when looking at the total relaxation in the composite over a period of 1800 seconds. For neat samples, there was a 73% reduction in modulus over a period of 1800 seconds. When 2.0 and 3.0 wt.% ANPs were incorporated into the CFRP composite, the reduction in modulus increased to 80% as shown in Figure 4.2. Mean relaxation modulus and stress-relaxation percentage of CFRP coupons incorporating ANPs are presented in Table 4.2. It is evident that ANPs significantly reduces the off-axis shear chord modulus and significantly increases off-axis stress-relaxation of CFRP.

Table 4.2: Relaxation modulus and stress-relaxation % for CFRP coupons incorporating ANPs.

CFRP type	E_0 (MPa)	E_f (MPa)	Stress-relaxation (%)
Neat	2408	641	73%
1.0 wt.% ANPs	2684	616	77%
2.0 wt.% ANPs	1597	321	80%
3.0 wt.% ANPs	1503	307	80%

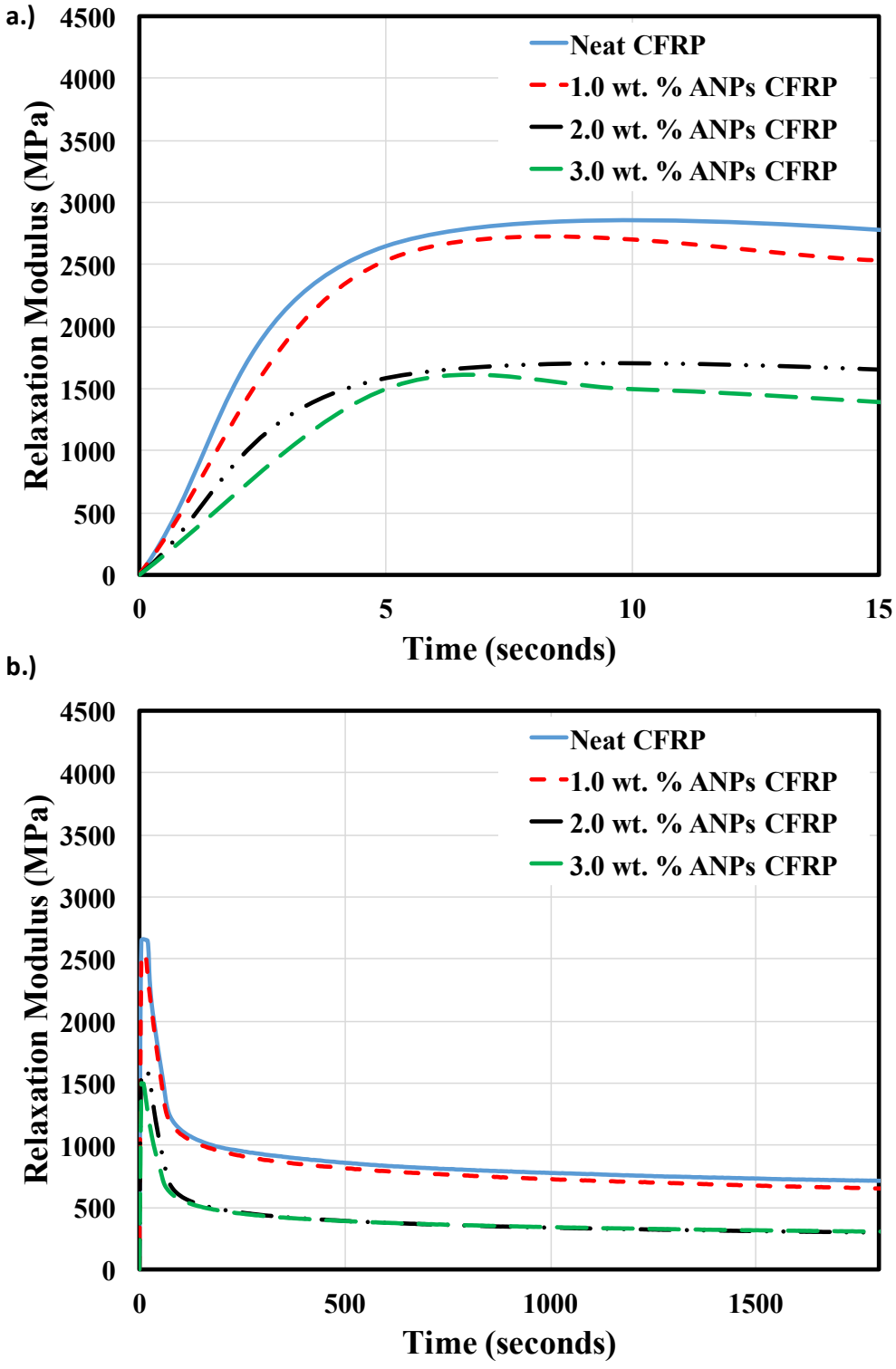

Figure 4.2: Initial loading behavior (a) of CFRP coupons incorporating ANPs, and (b) stress relaxation of CFRP coupons incorporating ANPs.

DMA tests of the ANPs-epoxy nanocomposite further confirmed the results from testing of the CFRP. As shown in Figure 4.3, neat epoxy had an initial modulus value of 914 MPa in comparison to a modulus of 604 MPa for 2.0 wt.% ANPs and 649 MPa for 3.0 wt.% ANPs. Figure 4.3 shows that the most significant stress relaxation occurs in the 2.0 and 3.0 wt.% ANPs-epoxy nanocomposite. Over a period of 1800 seconds, there was a 97% reduction in modulus observed in the 2.0 wt.% ANPs compared with an 87% reduction in modulus observed in the neat epoxy sample.

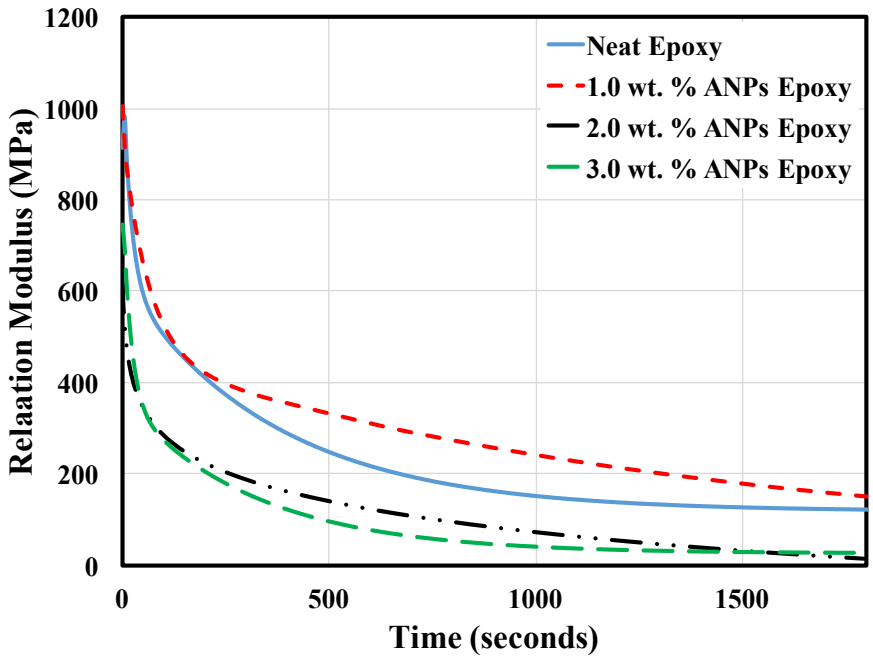

Figure 4.3: Stress relaxation of epoxy incorporating varying levels of ANPs

Analyzing DMA, it was found that incorporating ANPs affects the glass transition temperature (T_g) of the epoxy nanocomposite as presented in Table 4.3. Neat epoxy had the highest T_g at 61. 5°C and T_g was observed to decrease when 2.0 and 3.0 wt.% ANPs were incorporated into the matrix to 57.7°C and 56.8°C, respectively, representing a loss

in crosslinking due to the incorporating ANPs. Looking at the viscoelastic properties further, the storage modulus at 30°C for both the neat and epoxy incorporating 1.0 wt.% ANPs is higher than the epoxy incorporating 2.0 and 3.0 wt.% ANPs as shown in Figure 4.4.

Table 4.3: Glass-transition temperature of epoxy incorporating ANPs.

Epoxy type	T_g (°C)
Neat	61.5
1 wt.% ANPs	58.3
2 wt.% ANPs	57.7
3 wt.% ANPs	56.8

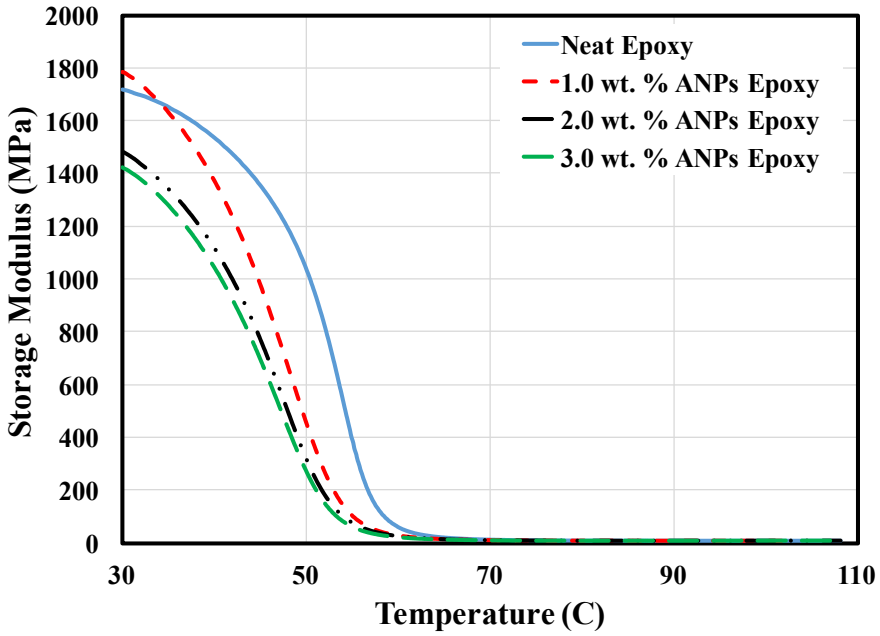

Figure 4.4: Storage modulus of epoxy incorporating varying levels of ANPs.

Investigation of the interaction between ANPs and the epoxy was performed by FTIR analysis. FTIR is utilized to observe chemical changes of the epoxy matrix after incorporating ANPs. Figure 4.5 shows the FTIR spectra of ANPs/epoxy nanocomposites in comparison with neat epoxy. The traditional epoxy absorption bands appearing in Figure

4.5 indicate bands corresponding to O–H groups (3200–3600 cm^{-1}), C–H (2850–2970 cm^{-1}), N–H of primary amines (1595–1630 cm^{-1}), ether (~1250 cm^{-1}), C–N (1040–1110 cm^{-1}), and epoxide ring (~830 cm^{-1}). The effect of incorporation of ANPs in the epoxy matrix is demonstrated by comparing the FTIR spectra of all ANP/epoxy nanocomposites with the neat epoxy. It can be observed that incorporating ANPs in the epoxy matrix increased intensities of both epoxide ring and primary amine N–H bands. The stretching band of hydroxyl groups is also significantly shifted to a lower wave number value (3415–3320 cm^{-1}) with a broader shape as shown in Figure 4.5. It is obvious that incorporation of ANPs shifts the O-H band from 3410 cm^{-1} (neat epoxy) to 3350 cm^{-1} for 1.0 and 2.0 wt.% and to 3320 cm^{-1} for 3.0 wt.%. This shift and band broadening could be attributed to the change in the curing behavior of the epoxy matrix due to the incorporated ANPs (Golru et al., 2014). It has been reported that the hydroxyl stretching vibration region with its broad complex band absorption is at about 3200–3600 cm^{-1}. This is explained by the wide shifting range based on the mode of hydroxyl group association, which depends on hydrogen bonding between hydroxyl and hydroxyl/carbonyl groups of different strength and hydrogen bonding of water molecules (Mikhaylova et. al., 2006). It has also been reported that a matrix having O–H groups could undergo two modes of hydrogen bonding; inter- and intramolecular hydrogen bonds between O–H groups based on the O-H location. Consequently, the presence of 1.0 or 2.0 wt.% ANPs in epoxy matrix shows a shifting O-H band to a lower wave number and broader shape. This could be explained by the effect of ANPs on epoxy curing, which results in lowering the cross-linking of the matrix affording the two different hydrogen bond interactions. As a result, and in comparing with neat epoxy, the produced ANPs/epoxy nanocomposites have lower crosslinking density

and consequently have different ratios of hydrogen bonding modes, which lead to different geometry with different force constants. Therefore, these different hydrogen bond modes of interaction are explained by shifting O-H wave number absorption. The above FTIR analysis explains the reduction in the shear modulus and the increase in the stress-relaxation of off-axis CFRP incorporating ANPs.

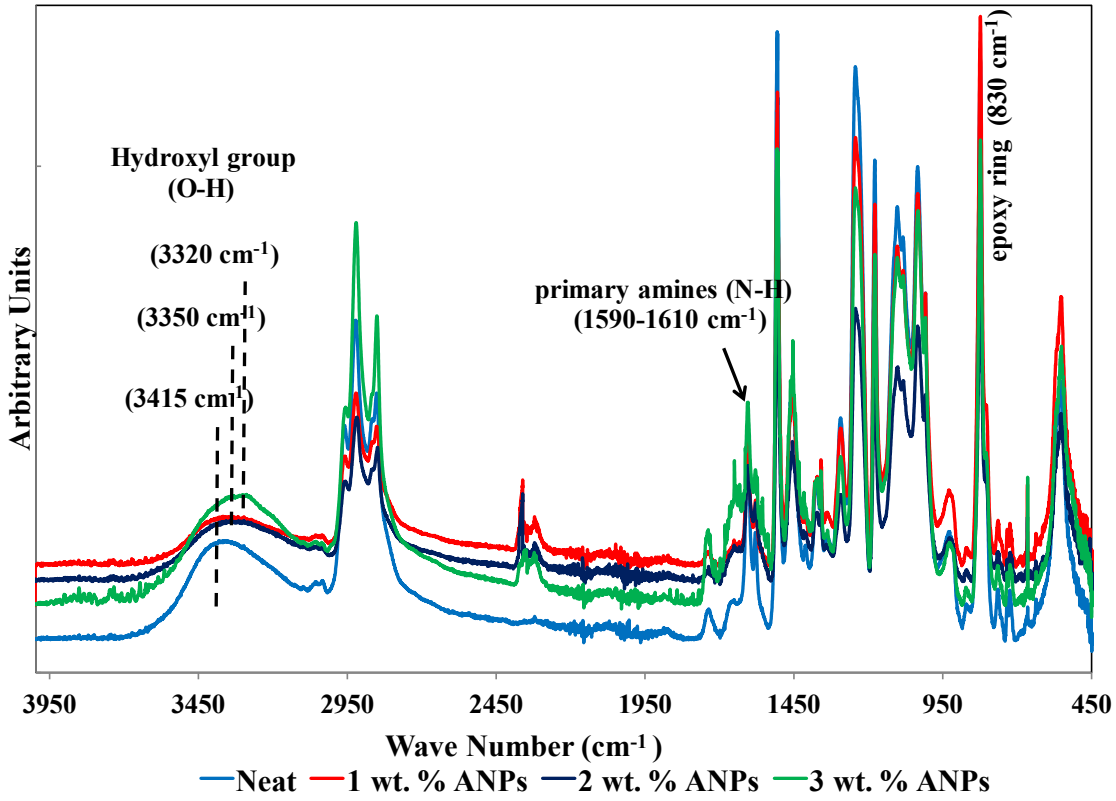

Figure 4.5: FTIR spectra of epoxy incorporating varying ANPs contents.

Using the modified rule of mixtures and Halpin-Tsai model, there should be an increasing trend of E_c as the concentration of ANPs increase in the epoxy, as predicted in Table 4.4. However, experimentally it was observed that while the modulus slightly increases when incorporating 1.0 wt.%, there is a significant decrease to 604 MPa when 2.0 wt.% ANPs are added. Interestingly, when 3.0 wt.% ANPs are added, the modulus of

the ANPs-epoxy nanocomposite increases to 649 MPa. The change in the epoxy curing with adding nanomaterials is not reflected in the rule of mixture or in the Halpin-Tsai model, which considers the nanoparticles only as fillers. On the contrary, it is apparent that ANPs affect epoxy polymerization at 2.0 wt.% and results in significant reduction of cross-linking and thus reduced stiffness and increased stress-relaxation. Additional nanoparticles content could start to act as fillers and thus slightly increase epoxy stiffness compared with the epoxy incorporating 2.0 wt.% ANPs. This explains why the modulus of epoxy started to increase again at 3.0 wt.% ANPs. The above analysis shows the inability of the current mixture models to predict the mechanical properties of polymers incorporating nanoparticles such as ANPs where those nanoparticles might interact chemically affect the polymerization process.

Table 4.4: Predicted initial stiffness (E_0) using analytical models versus experimental observations of epoxy nanocomposite.

Epoxy type	Experimental (MPa)	Modified rule of mixtures (MPa)	Halpin-Tsai (MPa)
Neat	879	879	879
1.0 wt.% ANPs	1005	984	889
2.0 wt.% ANPs	604	1093	899
3.0 wt.% ANPs	649	1204	900

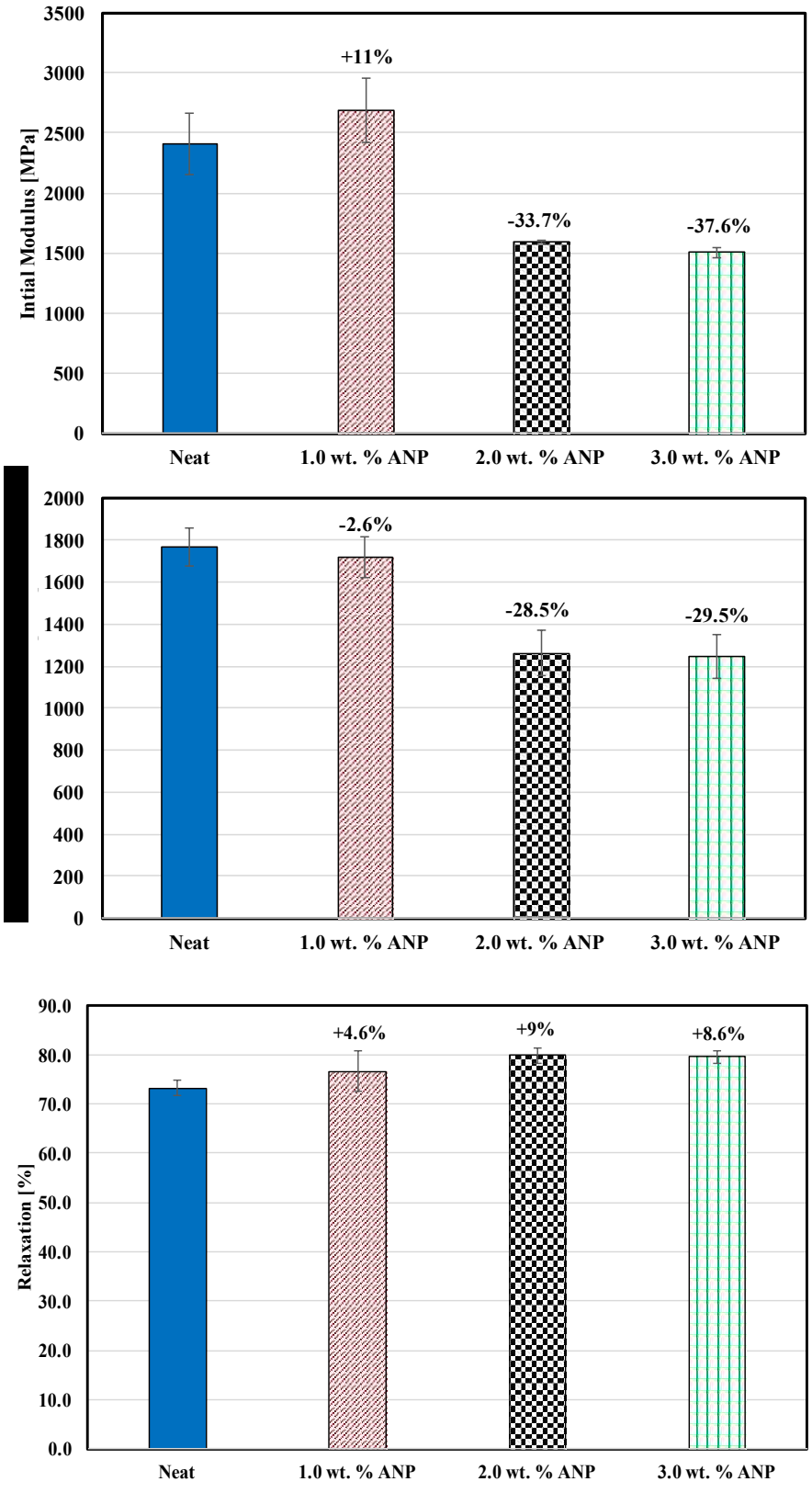

Figure 4.6: Stress-Relaxation of CFRP incorporating ANPs

4.3 Non-Functionalized Multi-Walled Carbon Nanotubes

Mechanical Behavior

There are several factors such as orientation, dispersion, and diameter of the MWCNTs that can impact the mechanical behavior of an epoxy nanocomposite when MWCNTs are incorporated. It has been proposed that when MWCNTs are dispersed in the epoxy, they can be considered as randomly oriented discontinuous fibers (Safadi et al., 2002; Mallick, 2008.) Under this assumption, the modulus of the MWCNT-epoxy nanocomposite, E_c, can be calculated using the following equations: (Mallick. 2008.)

$$\eta_L = \frac{(E_f/E_m) - 1}{(E_f/E_m) + 2(l_f/d_f)} \quad , \tag{4.4}$$

$$\eta_T = \frac{(E_f/E_m) - 1}{(E_f/E_m) + 2} \quad , \tag{4.5}$$

$$E_{11} = E_m \frac{1 + 2(l_f/d_f)\eta_L V_f}{1 - \eta_L V_f} \quad , \tag{4.6}$$

$$E_{22} = E_m \frac{1 + 2\eta_T V_f}{1 - \eta_T V_f} \quad \text{, and} \tag{4.7}$$

$$E_c = \left(\frac{3}{8}\right) E_{11} + \left(\frac{5}{8}\right) E_{22} \tag{4.8}$$

Where E_f and E_m are the moduli of the MWCNTs and epoxy, respectively. The outer diameter of the MWCNT is represented by d_f, the length by l_f, and MWCNT volume fraction as V_f. Using a density of 2.16 g/cm^3 for MWCNTs and a value of 1.08 g/cm^3 for the density of the epoxy, the MWCNTs by weight can be converted to MWCNTS volume

fraction, as shown in Table 4.5 (Omidi et al., 2010). A modulus value of 450 GPa was selected for the MWCNTs based on literature review and a value of 1.0 GPa was used for the neat epoxy based on experimental work (Montazeri et al., 2010).

Table 4.5: **Volume Fraction of MWCNTs**

W_f	V_f
0.5 wt. %	0.25%
1.0 wt. %	0.50%
1.5 wt. %	0.76%

Results and Discussion

Figure 4.7 shows the shear stress-shear strain behavior from testing off-axis CFRP coupons loaded in tension. Neat CFRP had the highest initial tangent modulus of 2408 MPa and a shear chord modulus of 1766 MPa. As shown in Table 4.6 and Table 4.7, when NF-MWCNTs are incorporated into the matrix, the initial tangent modulus and shear chord modulus decrease. When 0.5 wt. % NF-MWCNTs are incorporated, the initial tangent modulus decreases by 30% to 1694 MPa and the shear chord modulus decreased by 29% to 1026 MPa. Similarly, when 1.0 wt. % NF-MWCNTs are added to the matrix, it had an initial tangent modulus of 1294 MPa and a shear chord modulus of 1026 MPa, which is a decrease of 46% and 42%, respectively in comparison with neat CFRP. The greatest decrease in tangent modulus is seen when 1.5 wt. % NF-MWCNTs are incorporated into the matrix. The initial tangent modulus of the CFRP incorporating 1.5 wt. % NF-MWCNTs decreased by 58% and the shear chord modulus decreased by 49% to values of 1012 MPa and 895 MPa, respectively.

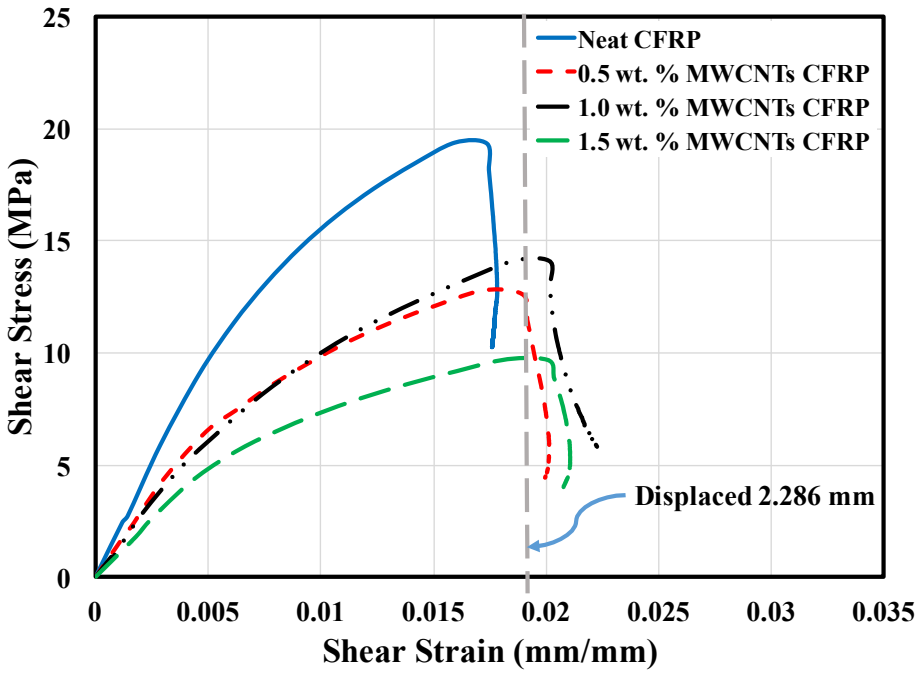

Figure 4.7: Stress-Strain relationship for CFRP coupons with varying levels of NF-MWCNTs (curves shown represent median out of 5 tested coupons)

Table 4.6: Mean off-axis shear modulus (± standard deviation) of CFRP coupons incorporating NF-MWCNTs

CFRP type	G_{12} (MPa)
Neat	1766±88.4
0.5 wt.% NF-MWCNTs	1259±114.0
1.0 wt.% NF-MWCNTs	1026±22.1
1.5 wt.% NF-MWCNTs	895±58.2

Table 4.7: Relaxation modulus and stress-relaxation % for CFRP coupons incorporating NF-MWCNTs.

CFRP type	E_0 (MPa)	E_f (MPa)	Stress-relaxation (%)
Neat	2408	641	73%
0.5 wt.% NF-MWCNTs	1693	260	85%
1.0 wt.% NF-MWCNTs	1294	263	80%
1.5 wt.% NF-MWCNTs	1012	181	82%

Looking at the stress-relaxation behavior of CFRP coupons incorporating NF-MWCNTs a similar trend can be observed as shown in Figure 4.8. Over a period of 1800 seconds, the neat CFRP coupons had a mean relaxation of 73% to a value of 641 MPa. When 0.5 wt. % NF-MWCNTs are incorporated in the matrix, the relaxation behavior behavior observed increase to a value of 85%, which is a 16% increase over neat epoxy. Similar behavior was observed when 1.0 wt. % and 1.5 wt. % NF-MWCNTs were added into the epoxy; 1.0 wt. % NF-MWCNTs CFRP showed a relaxation of 80% and incorporating 1.5 wt. % NF-MWCNTS showed a relaxation of 82% over 1800 seconds. Furthermore, not only is there a significant increase in the relaxation behavior observed in the CFRP over 1800 seconds, there is also a drastic reduction in modulus observed at 1800 seconds. The modulus of the CFRP at 1800 seconds when 0.5 wt. % NF-MWCNTs are incorporated is 260 MPa, which is a 59% lower than the modulus observed at 1800 seconds in comparison to the neat CFRP. Similarly, in the 1.0 wt. % and 1.5 wt. % NF-MWCNTs CFRP samples, the modulus at 1800 seconds was 262 MPa and 181 MPa, respectively. It shall be noted that while there was no statistical difference between the NF-MWCNTs incorporated CFRP samples, there was a significant difference between the neat CFRP and CFRP incorporating NF-MWCNTs.

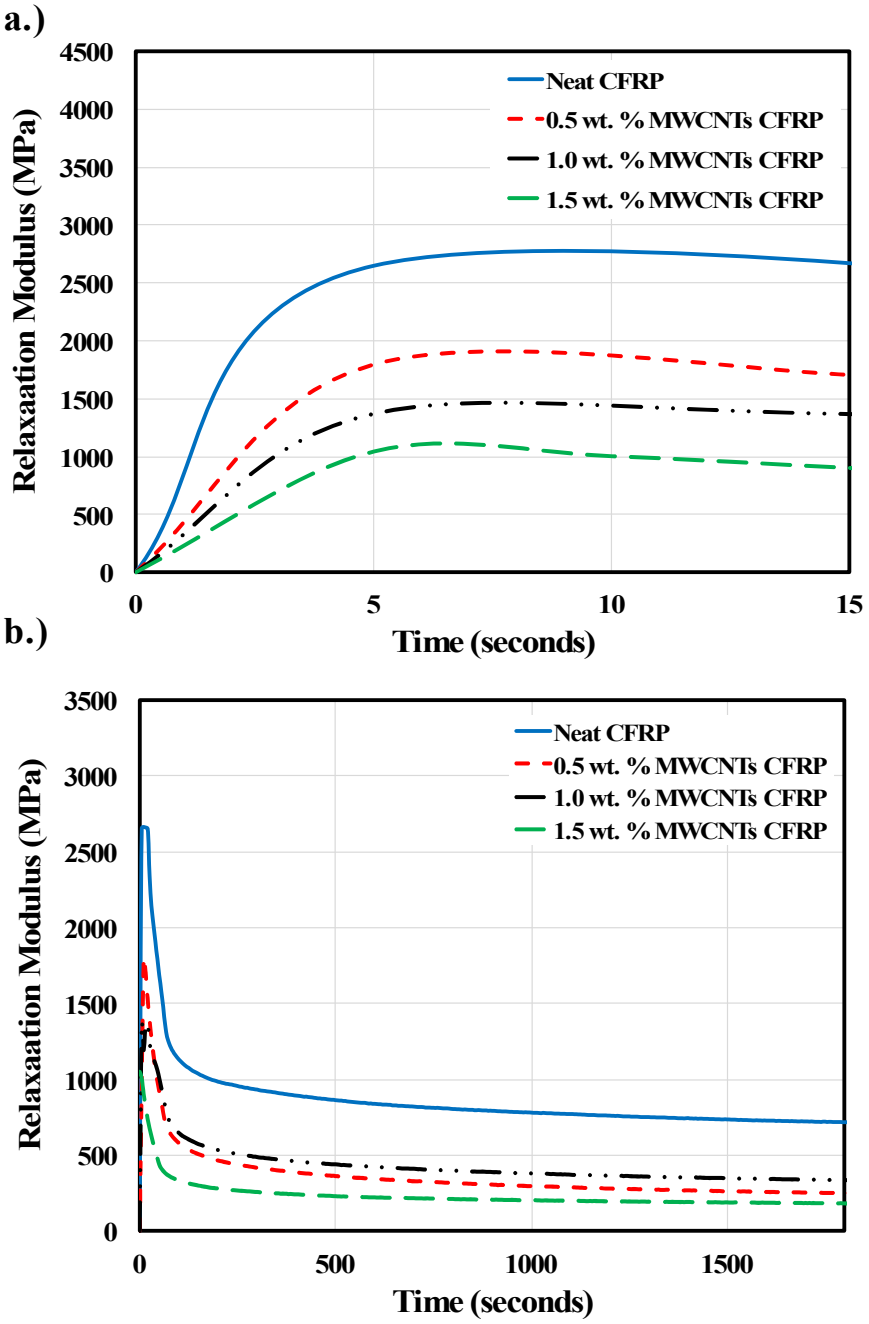

Figure 4.8: Initial loading behavior (a) of CFRP coupons incorporating NF-MWCNTs, and (b) stress relaxation of CFRP coupons incorporating NF-MWCNTs

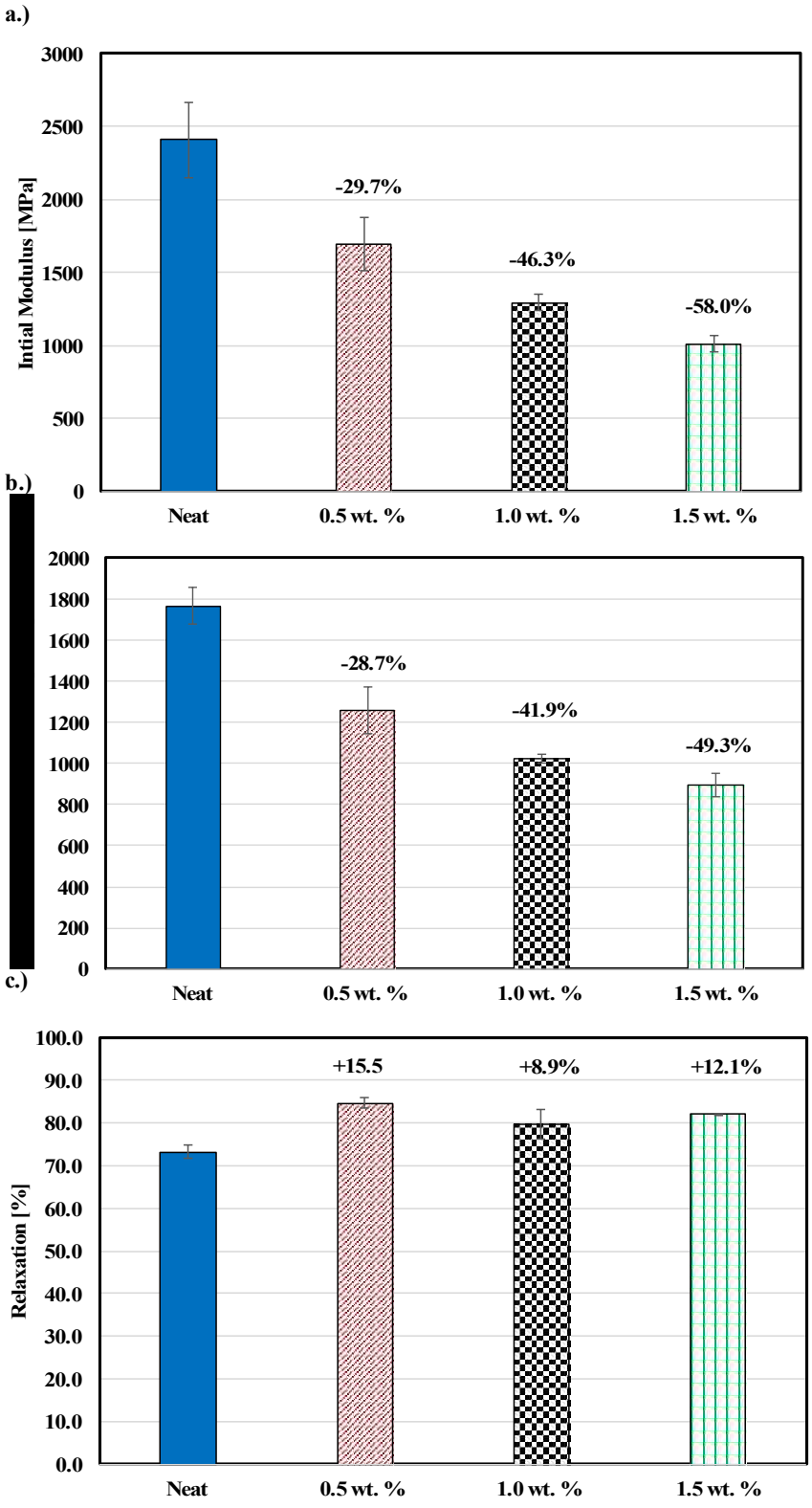

Figure 4.9: (a) Initial Modulus of CFRP incorporating NF-MWCNTs (b) Shear Chord Modulus of CFRP incorporating NF-MWCNTs (c) % Relaxation over 1800 seconds in CFRP incorporating NF-MWCNTs

As shown in Table 4.8, when incorporating NF-MWCNTs the glass transition temperature changed. The neat epoxy had the highest value of T_g at 61.5 °C. When 0.5 wt. %, 1.0 wt. %, and 1.5 wt. % NF-MWCNTs, the T_g decreased to values of 58.7 °C, 59.5 °C, and 57.4 °C, respectively. The most significant drop was seen when 1.5 wt. % NF-MWCNTs were added into the epoxy in which a drop of 4 °C was observed. It is presumed that at higher concentrations, the NF-MWCNTs agglomerate, causing a decrease in the T_g. Using time-temperature superposition theory (TTSP), mastercurves were generated for each concentration of NF-MWCNT, as shown in Figure 4.10. The neat epoxy had the highest initial modulus with a value of 879 MPa and experienced a reduction in modulus of 86% over 1800 seconds to a value of 121 MPa. When 0.5 wt. % and 1.0 wt. % NF-MWCNTs were incorporated in the matrix, there was an initial increase in the modulus of the epoxy to 1061 MPa and 1065 MPa, respectively. At 1800 seconds, the epoxy-nanocomposite samples incorporating 0.5 wt. % and 1.0 wt. % had modulus values of 94 MPa and 135 MPa, which is a decrease in initial modulus of 91% and 87%, respectively. When 1.5 wt. % NF-MWCNTs were incorporated in the matrix a significant decrease in the initial modulus of the epoxy was observed to a value of 560 MPa, which is a 43% reduction in comparison to the neat epoxy. At 1800 seconds, the 1.5 wt. % NF-MWCNTs epoxy sample had a modulus value of 20 MPa. This is a relaxation of 95%, which is an increase in relaxation over the neat epoxy by 8%.

Table 4.8: Glass-transition temperature of epoxy incorporating NF-MWCNTs.

Epoxy type	T_g (°C)
Neat	61.5
0.5 wt.% NF-MWCNTs	58.7
1.0 wt.% NF-MWCNTs	59.5
1.5 wt.% NF-MWCNTs	57.4

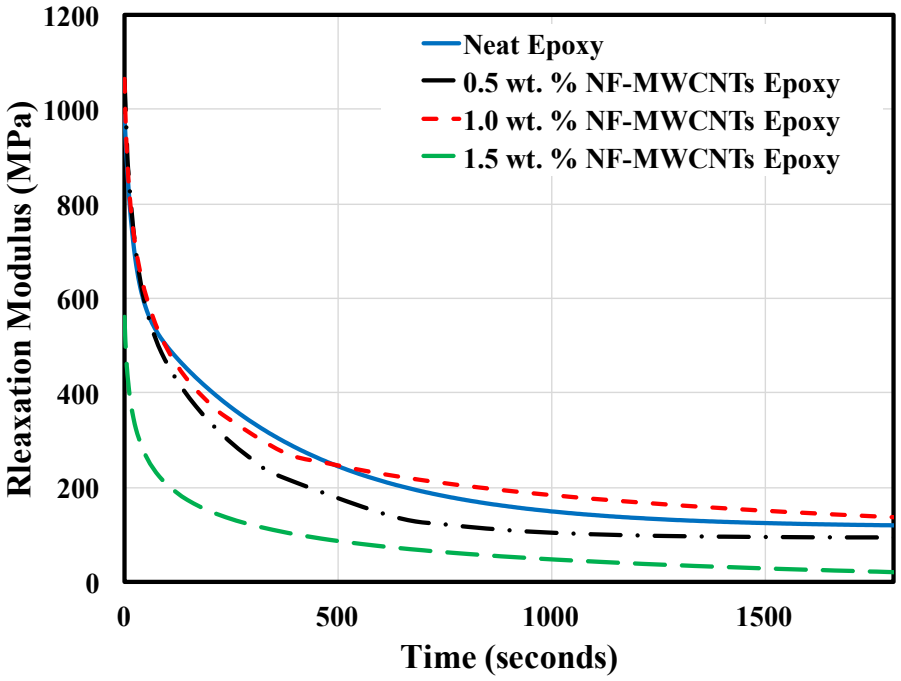

Figure 4.10: Stress relaxation mastercurves of epoxy-nanocomposite incorporating NF-MWCNTs

When considering the NF-MWCNTs as randomly oriented discontinuous fibers, the modulus of the epoxy-nanocomposite was calculated using Equations 4.4 - 4.8. As shown in Table 4.9, it is predicted that the modulus of the epoxy should continue to increase as more NF-MWCNTs are incorporated into the matrix. Experimentally it is shown that while there is a slight increase in the initial modulus of the epoxy-nanocomposite at weight concentrations of 0.5 % and 1.0%, the modulus significantly decreases when 1.5 wt. % NF-MWCNTs are incorporated in the matrix. This is in contrast to what the analytical model shows. This can be due to two different possibilities: (1) at higher values concentrations, the NF-MWCNTs tend to agglomerate and (2) the NF-MWCNTs inhibited a reaction taking place between the resin and the hardener, thus lowering the mechanical properties of the epoxy. This analysis shows that the current mechanical mixture models are unable

to properly predict the properties of epoxy when incorporating nanoparticles such as NF-MWCNTs, as they do not take into account that the nanoparticles do not always act as additional reinforcement, but rather can affect the polymerization process.

Table 4.9: Predicted initial modulus (E_0) using analytical model versus experimental observations of epoxy-nanocomposite

	Experimental (GPa)	Predicted (GPa)
Neat	0.88	0.88
0.5 wt. % NF-MWCNTs	1.01	0.98
1.0 wt. % NF-MWCNTs	1.06	1.22
1.5 wt. % NF-MWCNTs	0.56	1.56

4.3 Functionalized Multi-Walled Carbon Nanotubes

As shown in Figure 4.11, when incorporating F-MWCNTs there is a reduction in the initial modulus and shear chord modulus in comparison to neat CFRP. Additionally, it should be noted that the percent relaxation observed over a period of 1800 seconds increased. The initial modulus and shear chord modulus of neat CFRP was 2408 MPa and 1765 MPa, respectively. When 0.5 wt. % F-MWCNTs are incorporated into the matrix prior to fabrication, the initial modulus decreases to a value of 1802 MPa and the shear chord modulus decreases to 1449 MPa, which is a 25% decrease in the initial modulus and an 18% decrease in shear chord modulus. Furthermore, the percent relaxation observed over a period of 1800 seconds increased by 11% to a total relaxation observed of 81%. When 1.0 wt. % F-MWCNTs are incorporated into the matrix used in fabrication, the initial modulus and shear chord modulus values drop to 1664 MPa and 1326 MPa, respectively. This is a 31% and 25% decrease in modulus values in comparison to the neat CFRP, respectively. The percentage of relaxation observed over 1800 seconds increased to 79%, which is an increase of 7.6% over the neat CFRP coupons. Lastly, when 1.5 wt. % F-MWCNTs are incorporated in the matrix prior to fabrication, there is a reduction in the initial modulus and shear chord modulus to 1534 MPa and 1150 MPa, which is a 36% reduction and 35% reduction, respectively. The percent relaxation over 1800 seconds was 82%.

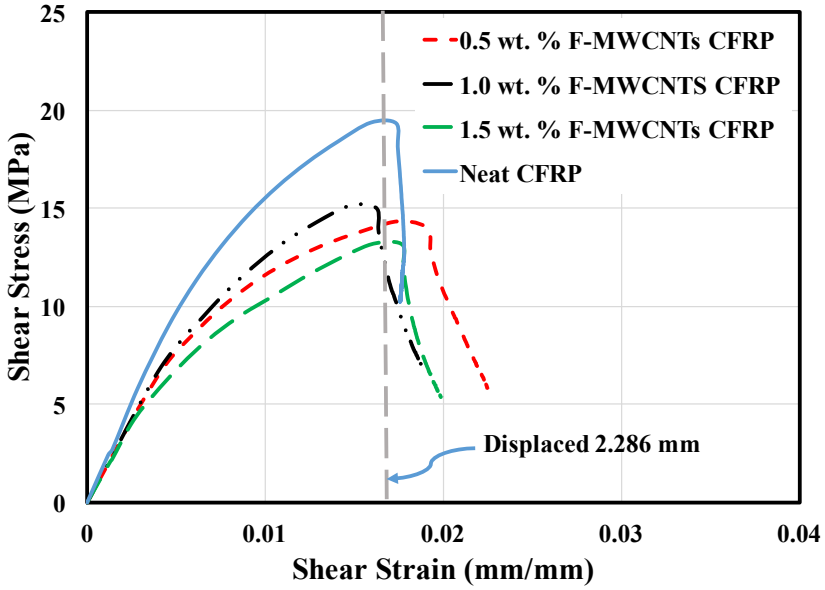

Figure 4.11: Stress-Strain relationship for CFRP coupons with varying contents of F-MWCNTs

Table 4.10: Mean off-axis shear modulus (± standard deviation) of CFRP coupons incorporating F-MWCNTs

CFRP type	G_{12} (MPa)
Neat	1766±88.4
0.5 wt.% F-MWCNTs	1449±16.8
1.0 wt.% F-MWCNTs	1326±83.1
1.5 wt.% F-MWCNTs	1150±86.2

Table 4.11: Relaxation modulus and stress-relaxation % for CFRP coupons incorporating F-MWCNTs.

CFRP type	E_0 (MPa)	E_f (MPa)	Stress-relaxation (%)
Neat	2408	641	73%
0.5 wt.% F-MWCNTs	1802	342	81%
1.0 wt.% F-MWCNTs	1664	353	79%
1.5 wt.% F-MWCNTs	1534	277	82%

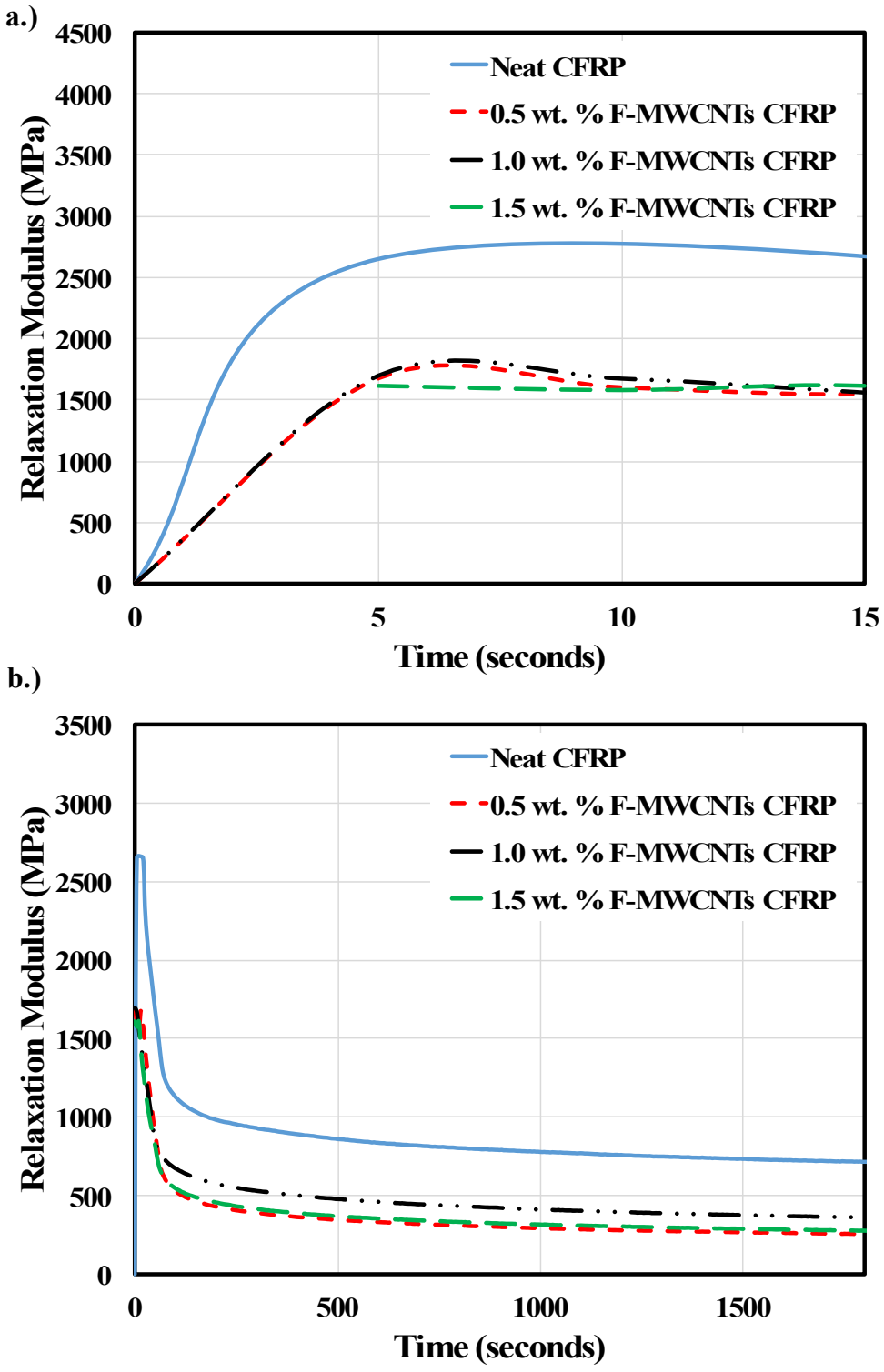

Figure 4.12: Initial loading behavior (a) of CFRP coupons incorporating F-MWCNTs, and (b) stress relaxation of CFRP coupons incorporating F-MWCNTs

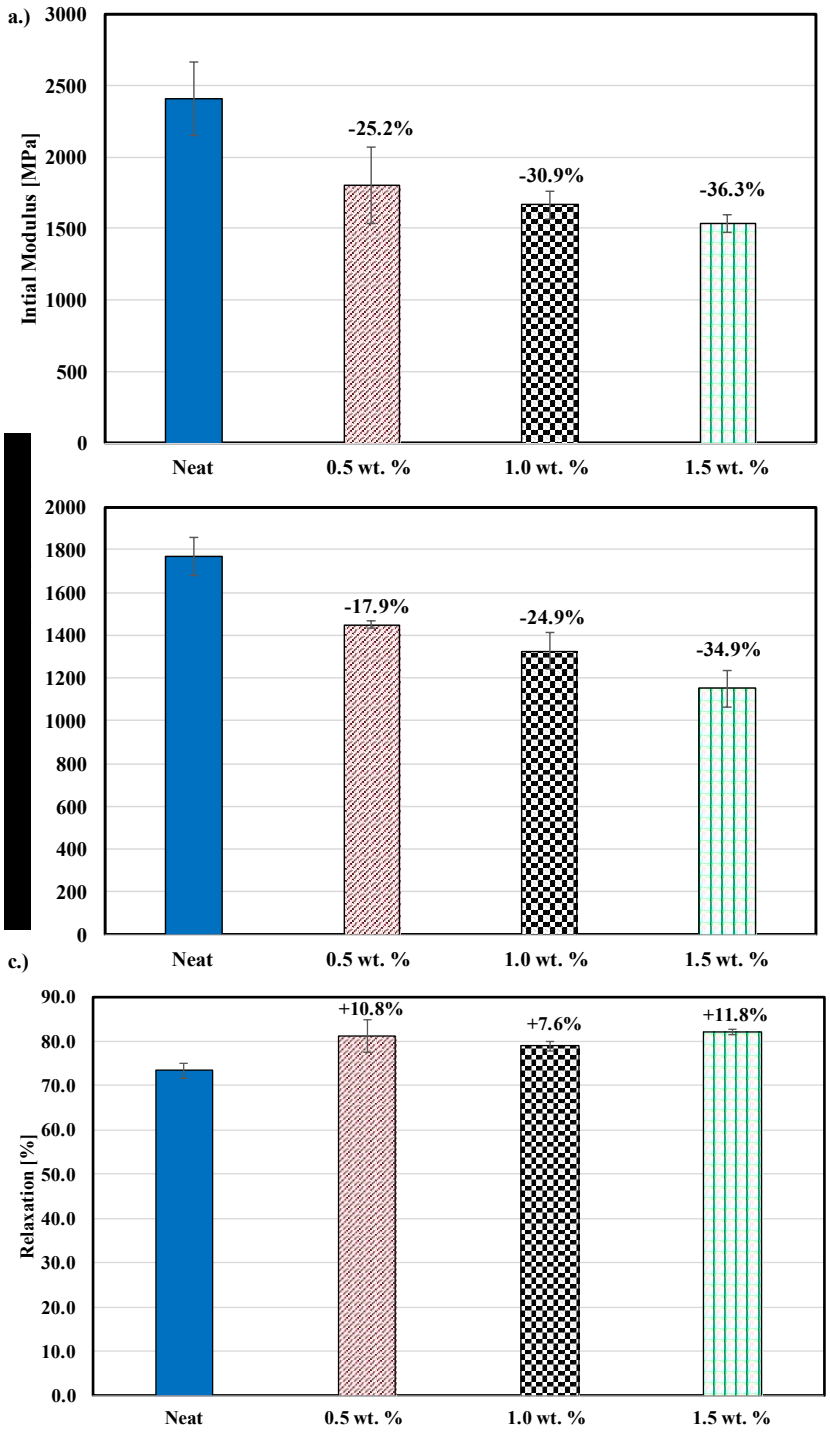

Figure 4.13: (a) Initial Modulus of CFRP incorporating F-MWCNTs (b) Shear Chord Modulus of CFRP incorporating F-MWCNTs (c) % Relaxation over 1800 seconds in CFRP incorporating F-MWCNTs

Looking at the DMA tests, similar behavior was observed in comparison to the CFRP tests. The neat epoxy had a median modulus value of 879 MPa, 0.5 wt. % F-MWCNTs-epoxy 917 MPa, 1.0 wt. % F-MWCNTs-epoxy 1038 MPa, 1.5 wt. % F-MWCNTs-epoxy 942 MPa. Over a period of 1800 seconds, the neat epoxy showed a relaxation of 86%, which is a decrease to a modulus value at 1800 seconds of 121 MPa. Over a period of 1800 seconds, when incorporating 0.5 wt. % F-MWCNTs, the modulus decreased to a value of 52 MPa, which is a total relaxation of 94%. In contrast to when using ANPs and NF-MWCNTs, which saw an increase in the relaxation behavior in the epoxy over 1800 seconds over all concentrations, there was no discernable difference in the relaxation of the epoxy when incorporating 1.0 wt. % and 1.5 wt. % F-MWCNTs in the epoxy. When incorporating 1.0 wt. % F-MWCNTs in the epoxy, the epoxy decreased to a value of 145 MPa, which is a relaxation of 86%. Similarly, when incorporating 1.5 wt. % F-MWCNTs in the epoxy, the modulus decreased to a value of 120 MPa over a period of 1800 seconds, which is a relaxation of 87%.

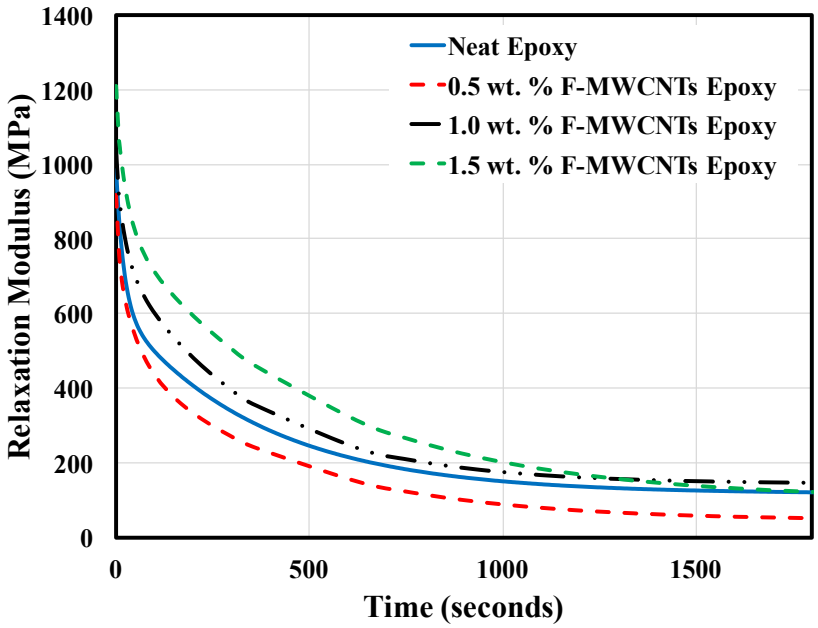

Figure 4.13: Stress relaxation mastercurves of epoxy-nanocomposite incorporating F-MWCNTs

This behavior is also reflected in the glass-transition temperature of the F-MWCNTs epoxy nanocomposite. When incorporating ANPs and NF-MWCNTs into the epoxy, there was a decrease seen in the glass-transition temperature, up to nearly 4 °C. Yet, when incorporating F-MWCNTs at 0.5, 1.0, and 1.5 wt. %, there was very little difference found between the neat epoxy and the samples incorporating nanomaterials. The neat epoxy had a T_g of 61.5 °C and the T_g decreased to values of 60.7 °C, 60.8 °C, and 60.4 °C when incorporating 0.5, 1.0, and 1.5 wt. % F-MWCNTs.

Table 4.12: Glass-transition temperature of epoxy incorporating F-MWCNTs.

Epoxy type	T_g (°C)
Neat	61.5
0.5 wt.% F-MWCNTs	60.7
1.0 wt.% F-MWCNTs	60.8
1.5 wt.% F-MWCNTs	60.4

CHAPTER 5 CONCLUSIONS AND RECOMMENDATIONS

An experimental study was conducted in order to investigate the benefits of incorporating nanomaterials at different weight concentrations on the stiffness and relaxation behavior of CFRP composites. Alumina nanoplatelets (ANPs), non-functionalized mutli-walled carbon nanotubes (NF-MWCNTs), and functionalized multi-walled carbon nanotubes (F-MWCNTs) were incorporated into the epoxy and used in CFRP lay-up. The CFRP coupons were tested in stress-relaxation. Initial modulus, shear-chord modulus, and modulus at 1800 seconds was compared and measured for all specimens. Furthermore, DMA and FTIR was utilized to understand the viscoelastic behavior and chemical changes in the epoxy.

5.1 Conclusions

5.1.1 ANPs-Epoxy Nanocomposites

In this study, the off-axis stiffness and stress relaxation behavior of off-axis CFRP composites incorporating ANPs were examined. Shear-strain, shear chord modulus and shear-stress, and relaxation modulus were determined for all specimens. A significant drop in shear chord modulus of CFRP by ~30% was observed when incorporating ANPs content of 2.0 and 3.0 wt.% into the epoxy matrix prior to CFRP fabrication. Furthermore, when incorporating 2.0 wt.% ANPs in the CFRP composites, stress-relaxation over a period of 1800 seconds increased by 10%.

DMA and FTIR observations were utilized to study the epoxy-ANPs nanocomposite. It was shown that the glass transition temperature of the epoxy-ANPs nanocomposite decreased when ANPs were incorporated in epoxy representing a loss in crosslinking of

the polymer matrix. Stress relaxation in master curves showed that when incorporating 2.0 wt.% ANPs into the epoxy, it resulted in a decrease in the initial modulus by 38% and an increase of stress-relaxation of 10% over a period of 1800 seconds. FTIR spectrograph showed that ANPs interrupted the epoxide ring and primary N-H bands increased when ANPs were added and there was a shift of the O-H band to a lower wave number. FTIR observations suggest ANPs inhibited the curing of the epoxy which lowered epoxy cross-linking and thus reduced elastic modulus and increased stress relaxation of both the epoxy matrix and off-axis response of CFRP. FTIR observations were able to provide a microstructural explanation of the macroscale behavior of the CFRP and epoxy in the stress-relaxation and DMA tests respectively. Finally, as the ANPs inhibited the resin from fully reacting with the hardener, traditional mechanical mixture models such as the modified rule of mixtures and Halpin-Tsai model were unable to accurately predict the modulus of the ANPs-epoxy nanocomposite. An alternative particupate composite model that is capable of accounting for the chemical effect of nanomaterials on the polymer matrix is needed to be able to accurately predict the mechanical properties of polymer nanocomposites.

5.1.2 NF-MWCNTs-Epoxy Nanocomposites

Stress relaxation behavior in CFRP composites incorporating NF-MWCNTs was investigated. The initial modulus, shear chord modulus, and relaxation modulus seconds was studied for all of the CFRP samples. It is shown that there is a significant decrease in the initial modulus and shear chord modulus beginning when 0.5 wt. % NF-MWCNTs are added into the matrix prior to CFRP fabrication of nearly ~30%. As the concentration of NF-MWCNTs increases to 1.0 wt. % and 1.5 wt. %, the initial modulus and shear chord

modulus values drop further to a value nearly 50% lower than that of the neat CFRP. Furthermore, when incorporating 0.5 wt. % NF-MWCNTs, the stress-relaxation behavior observed increased by 15% in comparison with the neat CFRP specimens.

DMA measurements showed that the glass transition temperature of the epoxy-nanocomposite decreased when NF-MWCNTs were incorporated in the epoxy which represents a reduction in crosslinking. The stress relaxation master curves showed that when 1.5 wt. % NF-MWCNTs are added into the polymer matrix, the initial modulus decreases by nearly 43% and the stress-relaxation behavior increases by 8% over a period of 1800 seconds. Lastly, it is shown that by assuming the NF-MWCNTs as randomly oriented discontinuous fibers, it does not appropriately predict the mechanical behavior of the epoxy-nanocomposite.

5.1.3 F-MWCNTs-Epoxy Nanocomposites

Stress relaxation behavior in CFRP composites incorporating F-MWCNTs was investigated. The initial modulus, shear chord modulus, and relaxation modulus seconds was studied for all of the CFRP samples. It is shown that there is a significant decrease in the initial modulus and shear chord modulus beginning when 0.5 wt. % F-MWCNTs are added into the matrix prior to CFRP fabrication of nearly ~25%. As the concentration of F-MWCNTs increases to 1.0 wt. % and 1.5 wt. %, the initial modulus and shear chord modulus values drop further to a value nearly 35% lower than that of the neat CFRP. Furthermore, when incorporating 0.5 wt. % F-MWCNTs, the stress-relaxation behavior observed increased by 10% in comparison with the neat CFRP specimens.

To study the epoxy-F-MWCNTs nanocomposites, DMA was utilized. It was shown that the glass transition temperature of the epoxy-nanocomposite decreased by 1 °C when F-MWCNTs were incorporated in the epoxy. The stress relaxation master curves showed that when 0.5 wt. % F-MWCNTs are added into the polymer matrix, the relaxation behavior increases by 8%. However, when incorporating 1.0 and 1.5 wt. % F-MWCNTs into the epoxy matrix, there was no change in the relaxation behavior over 1800 seconds in comparison with the neat epoxy, as it remained at nearly ~87% over 1800 seconds.

5.2 Recommendations and Future Work

These test methods of investigating the effect of nanomaterials on the stiffness and relaxation behavior of CFRP composites can be expanded to study the effect on the deployment in FRP composites. It is recommended that additional nanomaterials are studied, most notably at lower weight concentrations than were used in this research as well as hybrid-composites, such as using both NF-MWCNTs and F-MWCNTs in the same mixture. Furthermore, it is recommended to study the relaxation behavior of both the CFRP composite and epoxy-nanocomposites in three-point bending. This would eliminate potential clamping effects as well as issues due to the thermal expansion of the material.

Lastly, it is recommended to fabricate a tape-spring composite and measure the effect on deployment due to the incorporation of nanomaterials. This experimental work, combination with Abaqus, may allow for the composite to continue to be tailored to meet desired specifications.

CHAPTER 6 REFERENCES

Aboubakr SH, Kandil UF and Reda Taha M. Creep of epoxy-clay nanocomposite adhesive at the FRP interface: A multi-scale investigation. Int J Adhes Adhes. 54 (2014): 15–12.

ASTM D5687 / D5687M-95, Standard Guide for Preparation of Flat Composite Panels with Processing Guidelines for Specimen Preparation, ASTM International, West Conshohocken, PA, 2015, www.astm.org

ASTM D3171-15, Standard Test Methods for Constituent Content of Composite Materials, ASTM International, West Conshohocken, PA, 2015, www.astm.org

ASTM D3518 / D3518M-13, Standard Test Method for In-Plane Shear Response of Polymer Matrix Composite Materials by Tensile Test of a ±45° Laminate, ASTM International, West Conshohocken, PA, 2013, www.astm.org

ASTM D3039 / D3039M-14, Standard Test Method for Tensile Properties of Polymer Matrix Composite Materials, ASTM International, West Conshohocken, PA, 2014, www.astm.org

Al-Saleh, Mohammed H., and Uttandaraman Sundararaj. "Review of the Mechanical Properties of Carbon Nanofiber/Polymer Composites." *Composites Part A: Applied Science and Manufacturing* 42.12 (2011): 2126-142.

Arridge, R.G.C. *Mechanics of Polymers*. Oxford: Clarendon, 1975. Print.

Bortz DR, Merino C and Martin-Gullon I. Carbon nanofibers enhance the fracture toughness and fatigue performance of a structural epoxy system. Compos Sci Technol. 71: (2011) 315–8.

Brinkmeyer, Alex, Sergio Pellegrino, and Paul M. Weaver. "Effects of Long-Term Stowage on the Deployment of Bistable Tape Springs." *Journal of Applied Mechanics* 83.1 (2015): 011008.

Cox HL. The elasticity and strength of paper and other fibrous materials. British Journal of Applied Physics. 3 (1952) 725–9.

Esawi, A.M.K., K. Morsi, A. Sayed, M. Taher, and S. Lanka. "Effect of Carbon Nanotube (CNT) Content on the Mechanical Properties of CNT-reinforced Aluminium Composites." *Composites Science and Technology* 70.16 (2010): 2237-241.

Footdale, Joseph, and Thomas Murphey. "Structural Design of a CubeSat-Based Diffractive Optic Telescope." *52nd AIAA/ASME/ASCE/AHS/ASC Structures, Structural Dynamics and Materials Conference* (2011)

Footdale, Joseph N., Thomas W. Murphey, and Michael E. Peterson. "Design and Testing of Self-Deploying Membrane Optic Support Structure Using Rollable Composite

Tape Springs." *54th AIAA/ASME/ASCE/AHS/ASC Structures, Structural Dynamics, and Materials Conference* (2013)

Glaskova-Kuzmina, Tatiana, Andrey Aniskevich, Mauro Zarrelli, Alfonso Martone, and Michele Giordano. "Effect of Filler on the Creep Characteristics of Epoxy and Epoxy-based CFRPs Containing Multi-walled Carbon Nanotubes." *Composites Science and Technology* 100 (2014): 198-203.

Griffiths PR, De Haseth JA and Winefordner JD. Fourier Transform Infared Spectrometry, 2nd Edition. Hoboken, NJ: John Wiley & Sons, Inc., 2007.

Gojny, Florian H., Malte H.g. Wichmann, Bodo Fiedler, Wolfgang Bauhofer, and Karl Schulte. "Influence of Nano-modification on the Mechanical and Electrical Properties of Conventional Fibre-reinforced Composites." *Composites Part A: Applied Science and Manufacturing* 36.11 (2005): 1525-535.

Golru SS, Attar MM and Ramezanzedeh B. Studying the Influence of nano-Al2O3 particles on the corrosion performance an dihydrolytic degradation resistance of an epoxy/polyamide coating on AA-2015. Prog Org Coat. 77 (2014) 13915–9.

Guadagno, L., B. De Vivo, A. Di Bartolomeo, P. Lamberti, A. Sorrentino, V. Tucci, L. Vertuccio, and V. Vittoria. "Effect of Functionalization on the Thermo-mechanical and Electrical Behavior of Multi-Wall Carbon Nanotube/epoxy Composites." *Carbon* 49.6 (2011): 1919-930.

Guo, Chuangqi, Zhen Zheng, Qiren Zhu, and Xinling Wang. "Preparation and Characterization of Polyurethane/ZnO Nanoparticle Composites." *Polymer-Plastics Technology and Engineering* 46.12 (2007): 1161-166.

Guo, Peng, Xiaohong Chen, Xinchun Gao, Huaihe Song, and Heyun Shen. "Fabrication and Mechanical Properties of Well-dispersed Multiwalled Carbon Nanotubes/epoxy Composites." *Composites Science and Technology* 67.15-16 (2007): 3331-337.

Griffiths PR, De Haseth JA and Winefordner JD. Fourier Transform Infared Spectrometry, 2nd Edition. Hoboken, NJ: John Wiley & Sons, Inc., 2007.

Hussain, Manwar, Atsushi Nakahira, and Koichi Niihara. "Mechanical Property Improvement of Carbon Fiber Reinforced Epoxy Composites by Al2O3 Filler Dispersion." *Materials Letters* 26.3 (1996): 185-91.

Hyer, Michael W. *Stress Analysis of Fiber-reinforced Composite Materials*. Lancaster: Destech, 2009.

Iqbal, K., and S. Pellegrino. "Bi-stable Composite Shells." *41st Structures, Structural Dynamics, and Materials Conference and Exhibit* (2000)

Kar, Kamal K., S.D. Sharma, Prashant Kumar, and Akash Mohanty. "Stress Relaxation Behavior of Glass Fiber-reinforced Polyester Composites Prepared by the Newly Proposed Rubber Pressure Molding." *Polymer Composites* 29.10 (2008): 1077-097.

Kardar P, Ebrahimi M and Bastani S. Study the effect of nano-alumina particles on physical mechanical properties of UV cured epoxy acrylate via nano-indentation. Prog Org Coat. 62(3) (2008) 3215–5.

Khan A, Borowski E, Soliman E, and Reda Taha M. Examining energy dissipation of deployable aerospace composites using matrix viscoelasticity. American Society of Civil Engineering. 2017, In print.

Kim, Yeong K., and Scott R. White. "Stress Relaxation Behavior of 3501-6 Epoxy Resin during Cure." *Polymer Engineering & Science* 36.23 (1996): 2852-862.

Kuo MC, Tsai CM, et al. PEEK composites reinforced by nano-sized SiO2 and Al2O3 particulates. Mater Chem Phys. 90 (2005)1855–95.

Lim, S.H., K.Y. Zeng, and C.B. He. "Morphology, Tensile and Fracture Characteristics of Epoxy-alumina Nanocomposites." *Materials Science and Engineering: A* 527.21-22 (2010): 5670-676.

Ma, C.C.M, N.H. Tai, S.H. Wu, S.H. Lin, J.F. Wu, and J.M. Lin. "Creep Behavior of Carbon-fiber-reinforced Polyetheretherketone (PEEK) [±45] Laminated Composites (I)." *Composites Part B: Engineering* 28.4 (1997): 407-17.

Menard, Kevin P. *Dynamic Mechanical Analysis: A Practical Introduction*. Boca Raton, FL: CRC, 2008.

Meyers, Marc A., and Krishan Kumar Chawla. *Mechanical Behavior of Materials*. Cambridge: Cambridge UP, 2010.

Mikhaylova, Y. Adam, G., et al. Temperature-dependent FTIR spectroscopic and thermoanalytic studies of hydrogen bonding of hydroxyl (phenolic group) terminated hyperbranched aromatic polyesters. J. Mol. Struct. 788 (2006): 80–8.

Mobrem, Mehran, and Douglas Adams. "Deployment Analysis of the Lenticular Jointed Antennas Onboard the Mars Express Spacecraft." *Journal of Spacecraft and Rockets* 46.2 (2009): 394-402.

Montazeri, Arash, and Nasser Montazeri. "Viscoelastic and Mechanical Properties of Multi Walled Carbon Nanotube/epoxy Composites with Different Nanotube Content." *Materials & Design* 32.4 (2011): 2301-307.

Naous, Walid, Xiao-Yan Yu, Qing-Xin Zhang, Kimiyoshi Naito, and Yutaka Kagawa. "Morphology, Tensile Properties, and Fracture Toughness of Epoxy/Al2O3 Nanocomposites." *Journal of Polymer Science Part B: Polymer Physics* 44.10 (2006): 1466-473.

Omidi M, Rokni D.T. H, Milani AS, et al. Prediction of the mechanical characteristics of multi-walled carbon nanotube/epoxy composites using a new form of the rule of mixtures. Carbon. 2010; 48: 32185–28.

Omrani, Abdollah, Leonardo C. Simon, and Abbas A. Rostami. "The Effects of Alumina Nanoparticle on the Properties of an Epoxy Resin System." *Materials Chemistry and Physics* 114.1 (2009): 145-50.

Oskouei, A. V., and S. M. Taleie. "Experimental Investigation of Relaxation of Fiber-reinforced Polymer Composites." *Journal of Reinforced Plastics and Composites* 29.17 (2010): 2705-718.

Paul, D.r., and L.m. Robeson. "Polymer Nanotechnology: Nanocomposites." *Polymer* 49.15 (2008): 3187-204.

Perez, C.J., V.a. Alvarez, and A. Vasquez. "Creep Behaviour of Layered Silicate/starchâ□“polycaprolactone Blends Nanocomposites." *Materials Science and Engineering: A* 480.1-2 (2008): 259-65.

Peterson, Michael Edwin. *High Shear Strain Characterization of Plain-Weave Fiber Reinforced Lamina*. Thesis. University of New Mexico, 2015.

Qiao, P., E. J. Barbero, and J. F. Davalos. "On the Linear Viscoelasticity of Thin-Walled Laminated Composite Beams." *Journal of Composite Materials* 34.1 (2000): 39-68.

Rahman, M.M., S. Zainuddin, M.v. Hosur, C.J. Robertson, A. Kumar, J. Trovillion, and S. Jeelani. "Effect of NH2-MWCNTs on Crosslink Density of Epoxy Matrix and ILSS Properties of E-glass/epoxy Composites." *Composite Structures* 95 (2013): 213-21.

Rahman MM, Zainuddin S, Hosur MV, et al. Improvements in mechanical and thermo-mechnical properties of e-glass/epoxy composites using amino functionalized MWCNTs. Compos Struct. 94 (2012): 23975–406.

Skandani, A. Alipour, N. Masghouni, S. W. Case, D. J. Leo, and M. Al-Haik. "Enhanced Vibration Damping of Carbon Fibers-ZnO Nanorods Hybrid Composites." *Applied Physics Letters* 101.7 (2012): 073111.

Skandani, Amir Alipour, Ayoub Yari Boroujeni, Roozbeh Kalhor, Scott W. Case, and Marwan Al-Haik. "Viscoelastic Behavior of Epoxy/carbon Fiber/Zno Nano-rods Hybrid Composites." *Polymer Composites* 36.11 (2014): 1967-972.

Soliman, E., M. Al-Haik, and M. R. Taha. "On and Off-axis Tension Behavior of Fiber Reinforced Polymer Composites Incorporating Multi-Walled Carbon Nanotubes." *Journal of Composite Materials* 46.14 (2012): 1661-675.

Sullivan, J.l. "Measurement of Composite Creep." *Experimental Techniques* 15.5 (1991): 32-37.

TA Instruments, “Application of Time-Temperature Superposition Principles to DMA,” Thermal Analysis Applicaiotn Brief, TA-144, N.p., N.d., www.tainst.com

TA Instruments, “*DMA Q800 Specification*s,” N.p., 2010, Print.

TA Instruments, TS-63, “Determining the Optimum Sample Size for Testing a Film in the DMA 2980”, *Thermal Solutions*, www.tainst.com

TA Instruments, TS-64, “Measurement of the Glass Transition Temperature Using Dynamic Mechanical Analysis,” *Thermal Solutions,* www.tainst.com

TA Instruments, “*DMA Basics and Application Training,*” San Francisco, CA, 2015.

Thostenson, Erik T., Zhifeng Ren, and Tsu-Wei Chou. "Advances in the Science and Technology of Carbon Nanotubes and Their Composites: A Review." *Composites Science and Technology* 61.13 (2001): 1899-912.

Tibert, Gunnar. *Deployable Tensegrity Structures for Space Applications*. Diss. Royal Institute of Technology, 2002. Stockholm.

"Time-Temperature Superposition - a User's Guide." *Rheology Bulletin* 78.2 (2009): 16-31.

Tuttle, M. E., and H. F. Brinson. "Prediction of the Long-term Creep Compliance of General Composite Laminates." *Experimental Mechanics* 26.1 (1986): 89-102

Wetzel, Bernd, Frank Haupert, and Ming Qiu Zhang. "Epoxy Nanocomposites with High Mechanical and Tribological Performance." *Composites Science and Technology* 63.14 (2003): 2055-067.

Williams, Malcolm L., Robert F. Landel, and John D. Ferry. "The Temperature Dependence of Relaxation Mechanisms in Amorphous Polymers and Other Glass-forming Liquids." *Journal of the American Chemical Society* 77.14 (1955): 3701-707.

Wu, Chin-San, and Hsin-Tzu Liao. "Study on the Preparation and Characterization of Biodegradable Polylactide/multi-walled Carbon Nanotubes Nanocomposites." *Polymer* 48.15 (2007): 4449-458.

Kim, Yeong K., and Scott R. White. "Stress Relaxation Behavior of 3501-6 Epoxy Resin during Cure." *Polymer Engineering & Science* 36.23 (1996): 2852-862

Zhou, Yuanxin, Farhana Pervin, Shaik Jeelani, and P.K. Mallick. "Improvement in Mechanical Properties of Carbon Fabric-epoxy Composite Using Carbon Nanofibers." *Journal of Materials Processing Technology* 198.1-3 (2008): 445-53.